POLITECNICO

MILANO 1863

School of Industrial and Information Engineering

Master of Science in Biomedical Engineering

MASTER THESIS

HIP JOINT CENTRE ESTIMATION
BY NEURAL NETWORK PREDICTION

CANDIDATE:

Marta Ostini

ID. 883691

SUPERVISOR:

Prof. **Giancarlo Ferrigno**

CO-SUPERVISOR:

Prof. **Ricardo Machado Leite de Barros**

Prof. **Elena De Momi**

Academic Year 2017-2018

To my family and Andrea

for their love and support

Abstract

The accurate estimation of the hip joint centre is a basic requirement in clinical gait analysis as well as in preoperative planning of total hip arthroplasty and total knee arthroplasty. Clinical gait analysis is widely used to support clinical decision-making in case of gait dysfunction [1]. Gait deviations from the typical pattern are often characteristic of specific neurological or musculoskeletal pathologies. The importance of accurate HJC is due to the fact that its position influences both kinematics and kinetics. In surgical context, instead, the position of HJC is exploited for the correct placement of total hip and total knee prosthetic devices [2][3].

The most accurate hip joint centre localization is made using image-based methods. A 3D image of the patient is acquired using Computed Tomography (CT), Magnetic Resonance Imaging (MRI), Roentgen sterophotogrammetric analysis or other imaging techniques. Then the position of HJC is identified on medical images through manual localization or by calculating the centre of the best fitting sphere built on the segmented surface of the femoral head. These methods are expensive and, in case of usage of ionizing radiation, also invasive.

Image-less estimation of hip joint centre can be done according to different approaches: predictive methods and functional methods. When using functional methods, the HJC localization is computed with a kinematic approach that analyses the relative movement between femur and pelvis in a predefined reference system. Therefore, the subject is asked to perform a movement protocol, while an optical localization system measures the pose of the lower limb.

In predictive methods the position of the HJC is computed performing regression on specific anatomical quantities of the subject under analysis. These quantities are measured as tridimensional distances between accessible anatomical landmarks. The landmarks are identified through palpation. In this case the subject doesn't have to perform movements as in functional ones. Among predictive methods, the one proposed by Harrington et al. in [4], is considered the best performing [5], [6], therefore we used it as the gold standard.

The novel method for HJC prediction that we have developed in this thesis project is based on artificial neural networks (ANN). ANN is a machine learning technique that, after proper training, has intrinsic capability to model non-linear data and to find relationships between input and output parameters. Moreover, we wanted to include gender among input parameters and this was not possible while using a regression-based approach. Since HJC localization is a data-fitting problem, feedforward ANN with supervised training proved to be the best option.

The anthropometric measurements used for HJC estimation are clinical leg length (LL), pelvis width (PW) and pelvis depth (PD). To this parameters we added also age and gender. For network training and testing we used data from a dataset we found in literature [7]. Two more datasets, also found in literature, have been used for network performance analysis [4][8].

To obtain the best performing estimation algorithm we developed many networks, changing all the parameters that define network topology: number of nodes, number of hidden layers, number of inputs and number of outputs. Seven different networks have been developed and evaluated.

Algorithm 1. One network with full input parameters (PW, PD, LL, age, gender) and three outputs: HJCx, HJCy, HJCz (the coordinates x,y,z of HJC).

Algorithm 2. Three distinct networks, with full input parameters, each of which estimates one direction of hip joint centre (HJCx, HJCy, HJCz).

Algorithm 3. Three different networks. The first with full input parameter estimates

HJCy. The output of the first network (HJCy) is then used as input parameter, (together with LL, PW, PD, age and gender) for two other networks. This final two neural networks are used for HJCx and HJCz estimation.

Algorithm 4. Three networks are trained in the same way as in *Algorithm 3* but without including gender among input parameters.

Algorithm 5. Three networks are trained in the same way as *in Algorithm 3* but without including age among input parameters.

Algorithm 6 and *Algorithm 7.* For each algorithm, three networks are trained in the same way as *in Algorithm 3* with the addition of weight among input parameters.

The *Algorithms 1 to 5* have been implemented on imaging data and therefore in this case HJC estimation was carried out without considering fat and skin artefact. In the final part of Chapter 3 we simulated the presence of noise due to skin and fat layers between the anatomical landmarks located on the bones and the corresponding point identified through palpation. Two different noise simulations have been made. The first with random white noise, while the second with a random component plus a body mass index (BMI) dependent component. After noise addition, *Algorithm 6* and *Algorithm 7* have been implemented for HJC localization.

After algorithms implementation, the statistical analysis have been performed. We evaluated the *squared HJCx,y,z errors* and the distance between real and estimated HJC. In this analysis we validate the performance of our algorithms through the comparison with Harrington's algorithm. The most notable differences between the ANN algorithm and Harrington's can be spotted in the comparison of the 3D distance between real and estimated HJC. Considering the distance over two sets of data we had statistical evidence that our method increased the accuracy of HJC localization of 21-17% which correspond to average distance values of 5.9mm-9.3 mm, depending on used dataset. Harrington's average distance value were 7.5mm-11.2mm, depending on used dataset. The validation of the best performing method was carried out also on data with simulated noise. In this case, we proved an increase of approximately 19% in HJC

localization accuracy with mean value of 6.1mm.

Finally, we performed statistical analysis to evaluate the importance of including gender as input parameter. Although our data proved a certain relationship between the improvement in HJC localization and the use of gender as input parameter, our analysis on was not conclusive.

Sommario

La stima accurata del centro dell'articolazione dell'anca (Hip Jont Centre, HJC) è un requisito fondamentale nell'analisi clinica del cammino e nella pianificazione preoperatoria all'artroplastica totale di anca e di ginocchio. L'analisi del cammino è largamente utilizzata come supporto per il medico nel processo decisionale clinico in caso di disfunzioni nella deambulazione [1]. Le deviazioni dal modello tipico del cammino, infatti, sono spesso caratteristiche di patologie neurologiche o muscoloscheletriche specifiche. L'importanza della corretta localizzazione dell'HJC risiede nel fatto che la sua posizione influenza sia l'analisi cinematica che cinetica. Nel contesto chirurgico, invece, la posizione di HJC viene sfruttata per il corretto posizionamento delle protesi d'anca e di ginocchio [2], [3].

I metodi basati su immagini sono i più accurati nel lovalizzare il centro dell'articolazione dell'anca. Viene acquisita una immagine 3D del paziente utilizzando la tomografia computerizzata (CT), la risonanza magnetica (MRI), l'RX stereofotogrammetrico o altre tecniche di imaging. La posizione dell'HJC viene identificata sull'immagine da un operatore o è calcolata come il centro della sfera che meglio approssima la superficie segmentata della testa del femore.

La stima image-less del'HJC può essere effettuata secondo due diverse modalità: ultilizzando metodi predittivi o funzionali. Quando si utilizzano metodi funzionali, la posizione dell'HJC viene calcolata con un approccio cinematico che analizza il movimento relativo tra femore e la pelvi in un sistema di riferimento predefinito. Pertanto al soggetto viene chiesto di eseguire un protocollo di movimento, mentre un sistema di

localizzazione ottico misura la posa dei vari segmenti dell'arto inferiore.

Nei metodi predittivi la posizione dell'HJC viene calcolata eseguendo una regressione su specifiche misure anatomiche del paziente. Queste misure sono le distanze, in 3D, tra punti di riferimento anatomici accessibili, cioè che possono essere identificati attraverso la palpazione. Utilizzando i modelli predittivi il soggetto analizzato non deve eseguire movimenti come nel caso dei modelli funzionali. Tra i metodi predittivi, il metodo di Harrington, sviluppato in [4], è considerato il migliore [5], [6], quindi è stato utilizzato come gold standard.

Il nuovo metodo per la stima dell'HJC che abbiamo sviluppato in questo progetto di tesi è basato su reti neurali artificiali (ANN). Le reti neurali sono una tecnica di machine learning che ha la capacità intrinseca di stimare modelli per set di dati con relazioni non lineari, e quindi di trovare relazioni tra i parametri di input e output, dopo un una adeguata fase di training. La scelta di utilizzare le ANN è stata condizionata anche dalla decisione di includere il genere del soggetto tra i parametri di input. Questo non era possibile con l'utilizzo della regressione. Poiché la stima dell'HJC è un problema di fitting dei dati, l'utilizzo di reti neurali artificiali in configurazione feedforward e addestrate con training supervisionato si è dimostrata la scelta migliore.

Le misure antropometriche che sono sate utilizzate per la stima HJC sono la lunghezza della gamba (LL), la larghezza della pelvi (PW) e la profondità della pelvi (PD). A questi parametri abbiamo aggiunto anche età e genere. Per l'addestramento e il test della rete abbiamo utilizzato i dati appartenenti a un dataset presente in letteratura [7]. Sono stati utilizzati altri due set di dati, anch'essi toravati in letteratura, per l'analisi delle prestazioni delle reti neurali [4], [8].

Per ottenere l'algoritmo di stima più efficiente abbiamo sviluppato molte reti, modificando tutti i parametri che definiscono la topologia della rete: numero di nodi, numero di hidden layers, numero di ingressi e numero di uscite. Se si considera il numero di ingressi e uscite, sono state sviluppate cinque diverse reti neurali.

Algoritmo 1. È stata sviluppata una singola rete con in input LL, PW, PD, genere ed età, e tre output: HJCx, HJCy, HJCz (le coordinate x, y, z di HJC).

Algoritmo 2. Sono state sviluppate tre reti distinte, ciascuna con in input LL, PW, PD, genere e età. Ognuna delle tre reti stima una direzione del centro dell'articolazione dell'anca (HJCx, HJCy, HJCz).

Algoritmo 3. Sono state sviluppate tre diverse reti. La prima con tutti i parametri descritti sopra in input, che viene usata per la stima HJCy. L'output della prima rete (HJCy) viene quindi utilizzato come parametro di input (insieme a LL, PW, PD, età e genere) per addestrare altre due reti. Queste ultime due reti vengono utilizzate per la stima HJCx e HJCz.

Algoritmo 4. Sono state sviluppate tre diverse reti. Le reti sono state addestrate allo stesso modo dell'*Algoritmo 3*, ma senza includere il genere tra i parametri di input.

Algoritmo 5. Sono state sviluppate tre diverse reti. Le reti sono state addestrate allo stesso modo dell'*Algoritmo 3*, ma senza includere l'età tra i parametri di input.

Algoritmo 6 e *Algoritmo 7.* Per ciascuno dei due, sono state addestrate tre reti allo stesso modo dell'*Algoritmo 3*, ma con l'aggiunta del peso del soggetto analizzato tra i parametri di input.

Gli *Algoritmi da 1 a 5* sono stati implementati utilizzando i dati di imaging e quindi in questo caso la stima HJC è stata effettuata senza considerare gli artefatti dovuti alla presenza di tessuto adiposo e pelle. Nella parte finale del capitolo 3 è stata simulata la comoponente di rumore dovuta alla presenza di strati di pelle e tessuto adiposo tra i punti di riferimento anatomici situati sulle ossa e il punto corrispondente identificato attraverso la palpazione. Sono state effettuate due diverse simulazione del rumore. La prima con rumore bianco casuale, la seconda con un componente casuale e un componente dipendente dall'indice di massa corporea (BMI). Dopo la simulazione del rumore, sono stati implementati l'*Algoritmo 6* e l'*Algoritmo 7*.

Dopo l'implementazione degli algoritmi, sono state eseguite le analisi statistiche. Abbiamo valutato l'*errore quadratico di HJCx,y,z* e la *distanza*. Grazie a questa

analisi sono state valutate le prestazioni dei nostri algoritmi, confrontandoli con l'algoritmo di Harrington, che è considerato il gold standard per i modelli predittivi. Le differenze più evidenti tra gli algoritmi ANN e il modello di Harrington possono essere individuate nel confronto della distanza 3D tra HJC reale e stimato. Infatti, con riferimento a tale parametro, è stata riscontrata evidenza statistica che l'algoritmo basato su reti neurali ha aumentato l'accuratezza della localizzazione dell'HJC del 21-17% che corrisponde a un valore medio della distanza di 5,9 mm - 9,3 mm, a seconda del set di dati utilizzato. Il valore medio della distanza utilizzando il modello di Harrington era di 7,5mm-11,2mm, a seconda del set di dati utilizzato. È poi stata effettuata una valutazione sull'accuratezza della stima dell'HJC sui dati con simulazione degli artefatti dovuti alla pelle e allo strato adiposo. In questo caso è stata riscontrata evidenza statistica di un aumento del 19% circa nell'accuratezza della localizzazione dell'HJC con un valore medio di distanza, tra HJC reale e stimato, di 6,3mm.

Infine, è stata effettuata una analisi statistica per valutare l'importanza di includere il genere tra i parametri in input alle reti neurali. Non è stata riscontrata evidenza statistica di una correlazione tra il miglioramento della localizzazione HJC e l'uso del genere come parametro di input, tuttavia è stata trovata una relazione che riteniamo meriti ulteriori indagini.

Contents

Introduction

1.1 Introduction

The main target of this thesis is the development of a novel predictive method for the estimation of hip joint centre (HJC) position. An accurate localization of the centre of rotation of the joint is of primary importance for gait analysis and, in surgical context, for total hip and total knee arthroplasty. There are two approaches to compute the HJC: predictive methods and functional methods [6]. The first approach uses anatomical quantities as input parameters for the algorithm that estimates the HJC. The functional approach, instead, localize HJC exploiting kinematic relationships of relative movements of femur an pelvis. We decided to develop a predictive algorithm because it is more appropriate to apply predictive method in case the subject under study has neural disease, muscle-skeletal disability, or that underwent a surgical operation in the lower limb [1], due to the reduced range of hip joint motion. Functional methods, indeed, require the patient to perform wide movements with the lower limbs in order to be able to estimate the HJC, which is not necessary when using predictive method. HJC estimation is also widely used in gait analysis, which means that, in case of functional method, it demands the subject to perform the aforementioned movements before the analysis, and only after that the acquisition of gait patterns is performed. This increases the overall

acquisition time for the patient compared to predictive methods. Of course a higher time performing task may cause muscle soreness and so the gait pattern acquired may not be the same as without fatigue. Among the predictive methods the one that is considered to perform better, according to many study [5], [6], is Harringthon's algorithm [4]. The algorithm proposed by Harrington uses three anatomical measurements as parameters for HJC estimation: pelvis width, pelvis depth and clinical leg length.

1.2 Thesis Contribution and Organization

We propose an HJC estimation method based on artificial neural networks. This approach permits the modelling of complex data as well the inclusion of binary information among the parameters used for HJC estimation. We exploited this additional degree of freedom provided by ANN by including the gender (male/female) of the patients. We also added the age of the subject under analysis to the parameters used for estimation. In the last part of Chapter 3 we will also perform a simulation of fat and skin artefact, and therefore, we will included also weight among the parameter for the estimation of HJC. In the final part of Chapter 4 we will investigate the importance of including age and gender among input parameters. The main contribution of this thesis is that we will significantly improve the accuracy of Harrington's method in terms of estimation error. We will also perform an analysis with soft tissue artefact that will also prove better performance compare to other predictive methods.

The thesis is organized as follows. In Chapter 2 we provide a basic background on HJC estimation and its importance in the fields of computer aided surgery and in gait analysis. We then give the description of existing functional and predictive methods, as well as we introduce some useful theory and notation regarding artificial neural networks. The core of the thesis is in Chapter 3, were our mathematical model for HJC estimation is developed and tested. In Chapter 4, we perform a statistical analysis to compare the performance of our algorithm with Harrington's data. Finally, conclusions

are drawn in Chapter 5.

The first part of this thesis project was carried out at the *Laboratorio de Instrumentação para Biomecânica* (Biomechanical Instumentation Laboratory) of Universidad Estadual de Campinas under the monitoring of Prof. Ricardo M.L. de Barros. The second part of the thesis was developed at the *NEARLab* of Politecnico di Milano under the supervision of Prof. Giancarlo Ferrigno and Prof. Elena De Momi.

2

Background

This chapter is devoted to the necessary background material for the rest of the thesis. In Section 2.1 we introduce the importance of HJC localization and how a mislocation of it's position can lead to wrong deduction in human motion analysis and in computer assisted orthopaedic systems (CAOS). Then, in Section 2.2 and 2.3 we will give a short description of the already existing predictive and functional methods for HJC estimation. Finally, in section 2.4 a brief description of the mathematical model of the neural network is given.

2.1 Application of HJC localization

The accurate estimation of the hip joint centre is a basic requirement in lower limb movement analysis and in computer assisted orthopaedic procedures for total hip arthroplasty (THA) and total knee arthroplasty (TKA).

In gait analysis, precise location of the HJC is important as it influences both kinematics and kinetics [9]. The most used technique for gait analysis consists in the placement of markers, that may be active or passive, on the subject under analysis. The markers are acquired by a stereophotogrammetric system which provides 3D position of the markers in time, while the subject is performing movements. Often, force plates are used

to measure external forces. An example of a stereophotogrammetric system for gait analysis is shown in Fig. 2.1. The markers are usually placed on relevant anatomical
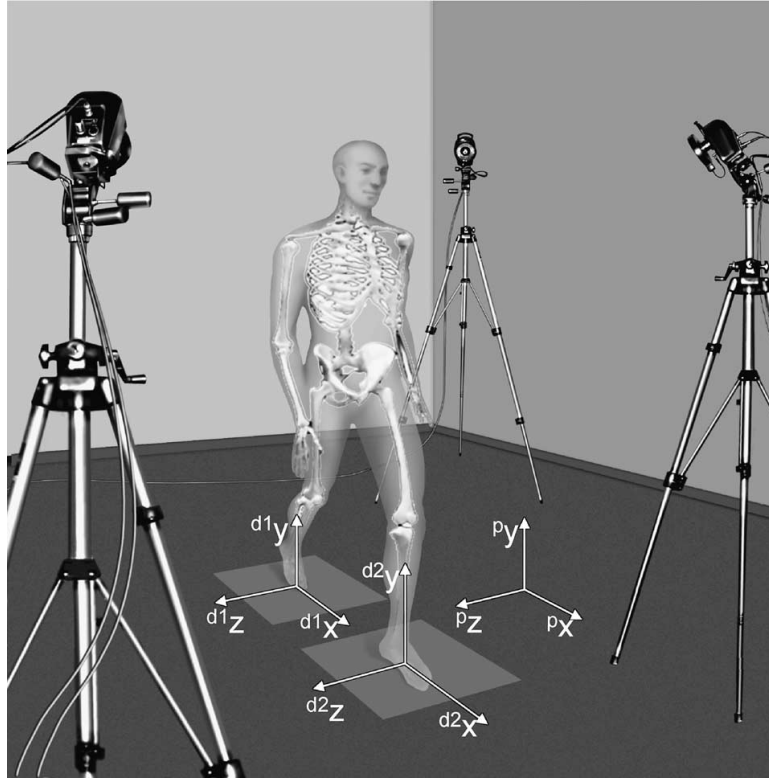
Figure 2.1: The human movement analysis laboratory. Basic measurement instruments are depicted together with their systems of axes (p: photogrammetry; d: dynamometry) [10].

landmarks and, if they can be palpated, the reliability of marker placement depends mainly on the operator experience and on the dimension of the bony prominence itself. When performing a complete gait analysis, the positions of some non-palpable anatomic landmark are of strong interest and therefore, these anatomic landmarks are usually estimated using indirect methods [11]. Among internal anatomic landmarks the HJC (i.e. the centre of femur head) is of high importance because it is the point with respect to which hip and knee joint momentum are calculated. There are two main categories of algorithms for HJC estimation: functional and predictive methods. The first one show

the smallest error, but they are not always applicable due to and inadequate range of hip joint motion in several patient populations [5], [11]. Clinical gait analysis consists in acquiring and interpreting biomechanical measurements of walking in order to support clinical decision-making in case of gait dysfunction [12]. Gait deviations from typical pattern are often characteristic of specific neurological or musculoskeletal pathologies. Baker [1] identified four potential reasons for performing a clinical gait analysis: diagnosis, evaluation, monitoring and prediction. It must be said that it is quite rare that a diagnosis is based only on gait analysis, and so at present day most common use is for evaluation of patients with a known condition prior to planning treatment for monitoring progress. Although the prediction of the outcome of patient-specific surgical operation would be extremely useful the development of such an algorithm is complex due to subject variability and this makes prediction difficult to use in practice.

Figure 2.2: (Left) The individual components of a total hip replacement. (Center) The components merged into an implant. (Right) The implant as it fits into the hip [13].

In CAOS applications, the estimation of the HJC is a fundamental planning phase for surgical procedures that operate both directly on the hip joint (total hip arthroplasty), and on the knee joint (total knee replacement or total knee arthroplasty).

It has been demonstrated [14] that improper HJC location can affect hip loading, angles, momentum and powers calculation acting at the hip joint leading to inaccurate evaluation on prosthetic device placement. The components of a total hip prosthetic device are femoral steam (metallic), femoral head (metallic), plastic liner (polyethylene) and acetabular component (metallic) The imprecise implantation of the acetabular component, i.e. placement out of the Lewinnek et al. [15] safe zone, combined with the unpredictability of uncemented stem anteversion may be the reason for dislocation after total hip arthroplasty [2], which is one of the most common complication after total hip arthroplasty.
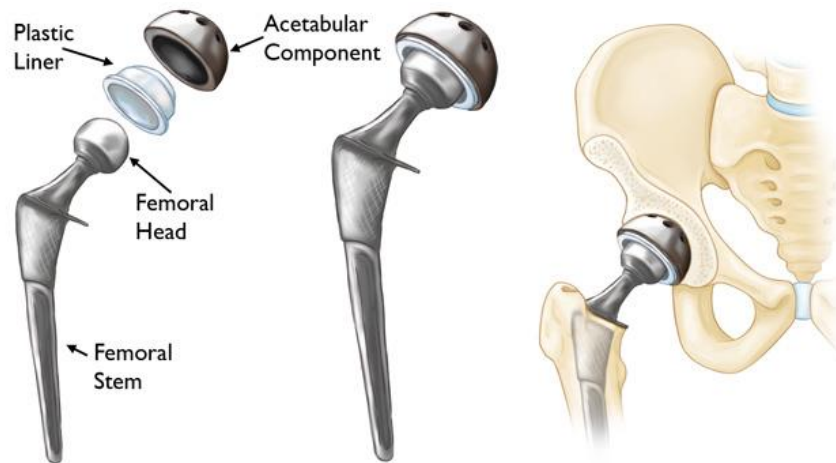

Figure 2.3: (Left) The individual components of a total knee replacement. (Center) The components merged into an implant. (Right) The implant as it fits into the knee.

In total knee arthroplasty, the surgeon completely replace the damaged joint with a total prosthesis formed by the following components: femoral component (metallic), tibial component (metallic) and tibial insert (in polyethylene). Visual representation of the device in Fig.2.3. The reference for the correct alignment of the prosthetic components is the mechanical axis of the lower limb, which identifies the direction of transmission of the load forces through the knee joint [3]. The mechanical axis is defined as the line joining hip joint centre with the centre of the tibiotalar joint. The mechanical axes of the femur is defined as the line that joins HJC and knee centre while tibia's

mechanical axis is defined as the line that joins knee centre and ankle joint centre. In healthy subjects, in upright position, the mechanical axis passes from a point 5-10mm from the centre of the knee.

2.2   Image based methods

The hip joint centre (HJC) is defined by processing patient-specific images obtained by Computed Tomography (CT), Magnetic Resonance Imaging (MRI), sterephotogrammetric RX or other imaging techniques. The position of HJC is identified on the image data through manual localization or by calculating the center of the best fitting sphere built on the segmented surface of the femoral head. In the case of non-automatic HJC localization (i.e. position identified by the operator Fig. 2.4), an estimation of the accuracy of the method was made by Reiko et al. [7] who concluded that the accuracy, compared to sphere fitting, was 1.1mm (SD: 0.3mm). The repeatability intra-assessor was $\pm$ 1.4, $\pm$ 1.5 and $\pm$ 1.8 mm for the posterior-anterior, medial-lateral, and inferior-superior directions respectively. Image based methods are expensive and, in case of use of X-ray images, have a non-negligible level of invasiveness due to the patient's exposure to radiation.
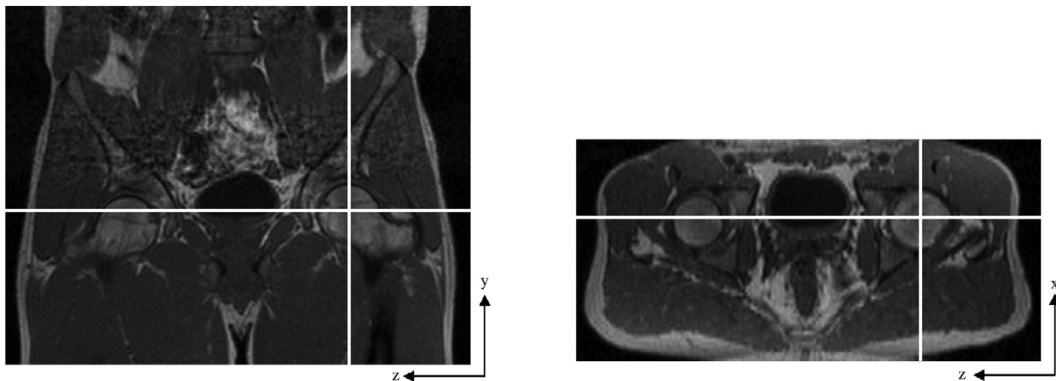

Figure 2.4: Example of manual localization of HJC on MRI images. Picture from [4].

Computer-assisted orthopaedic surgery (CAOS) has been developed for more accurate positioning of implants during the THA. In the context of total hip arthroplasty, the accurate positioning of implants is fundamental to achieve a good clinical outcome. To help surgeons in implant placement diverse CAOS systems have been developed. There are three main categories: passive, semi-active, and active systems. Among passive system, navigation systems are the most widely used and they basically provide the surgeon with necessary informations during surgery. Navigation can be made with different imaging techniques, like CT-scan, or, in order to reduce the radiation dose for the patient, with imageless systems [2]. Active and semi-active systems instead are robot-assisted system developed to help the surgeons both, providing informations and supporting prosthetic device implantation. Active systems perform partial or complete prothesis placement as programmed preoperatively. In semi-active system, the robotic arm is moved by the surgeon's hand by holding surgical tools, but it is kept constrained in preoperatively set boundaries. Among semiactive systems the MAKOplasty®system is one of the best performing for CAOS. To perform THA with MAKOplasty®first a pre-surgical CT-scan must be acquired. In the operative phase two pins should be fixed one on the bony surface, one of the greater trochanter and the other above the rim of the acetabular component on the bony pelvic. To assure correct superimposition of preoperative images and operation reference frame, femur and pelvis registration is done. Femur registration is made by touching with special tool on thirtytwo required points on the proximal femoral head. Pelvis registration is also made by touching, using special tool, the bone surface of the acetabulum on the thirty-two points identified by the software. Finally the surgeon can ream the acetabulum until he match the final socket size, however, the reamer remains constrained to the preoperative plan and avoids going "out of bounds" in the superior, medial or anterior-posterior directions.

At NEARLab we performed a simulation of the registration phase, of both pelivis and femur, using Polaris VICRA®sytem on a phantom. The phantom is made in rigid foam and is composed of two bony segments representing the pelvis and the femur.

Figure 2.5: On the left, femur with DRF_f rigidly linked plus pointer tool. On the right, pelvis with DRF_p rigidly linked plus pointer tool
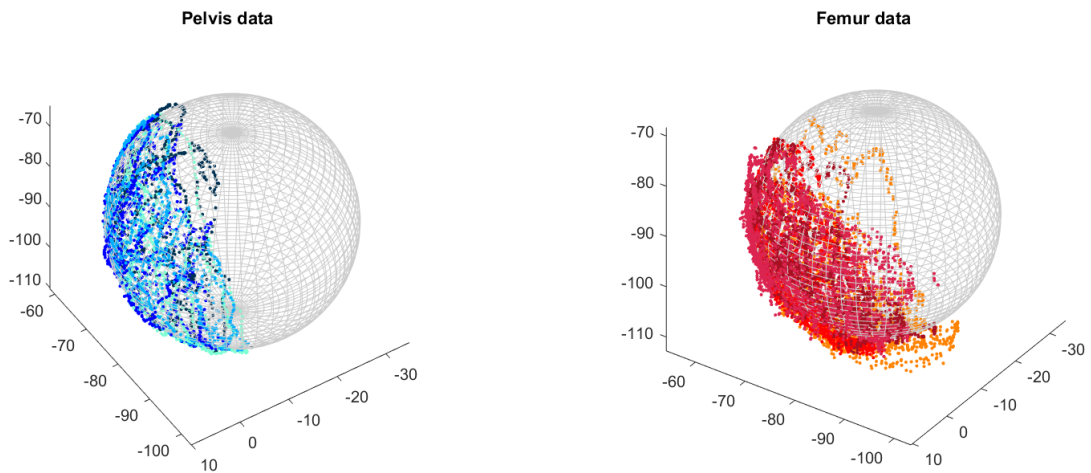
Figure 2.6: Data acquired, with VICRA®system, using the pointer tool on the acetabulum and femoral head surface.

VICRA®acquisition system tracks the 3D position and orientation of active or passive markers attached to surgical tools. The latter are rigid body with four passive markers each; the markers are placed so that it is possible to identify univocally position and orientation of the tool in space, therefore they are also called datum reference frame (DRF).

We used three different tools: two of them were rigidly linked one to the phantom pelvis (DRF_p) and the other to the femur (DRF_f), the third is a pointer tool that was used to collect point on the surface of femur head and acetabulum Fig. 2.5. All data are col-
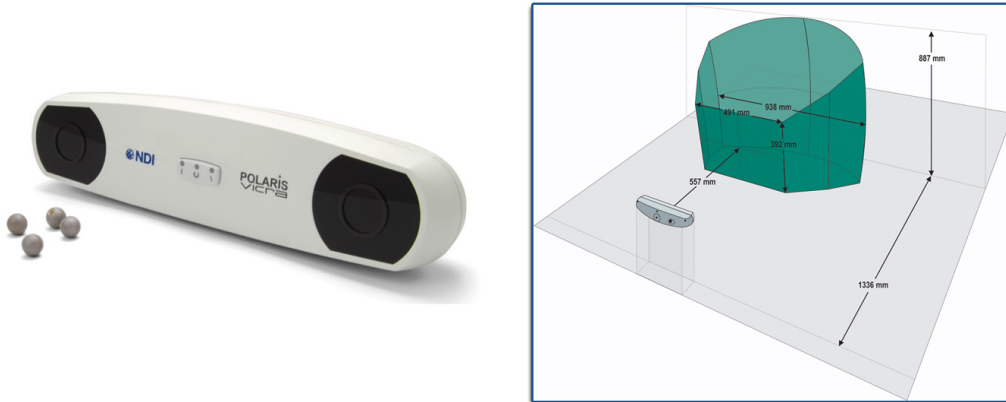
Figure 2.7: Camera of VICRA®Polaris acquisition system on the left and and image of VICRA®working space on the right.

lected in the camera reference frame, then data of femur head surface are rototranslated into femur's DRF_f and data of acetabulum surface into pelvis DRF_p. A static image of pelvis and femur with the femur head properly place in the acetabulum is also acquired. This last acquisition was made to be able to express femur head data in pelvic DRF_p, in order to make a comparison of the hip joint centres obtained by the two set of data. The HJC computed from femur head data was in position -80.0mm -13.4mm -89.0mm (x,y,z direction respectively), while it was in position -81.0mm -12.8mm -87.0mm (x,y,z direction respectively) when computed from acetabulum data, all the data expressed in DRF_p. This corresponds to a distance between the two HJC of 2.3mm consistent with what found in literature [7]. We consider the real HJC position as the mean position of the two: -80.5mm -13.1mm -88.0mm (x,y,z direction respectively).

2.3   Predictive methods for HJC localization

In predictive methods the position of the HJC is calculated with a regression-based approach on specific anatomical patient quantities, estimated from anthropometric data collections. To measure the specific anatomical quantities of the subject, some accessible anatomical landmark are identified through palpation and in correspondence of each of them a skin marker, for motion analysis applications, is placed. These HJC localization methodologies are less expensive and reduce the total analysis time with respect to image-based anatomical methods and functional methods. Furthermore, they are less invasive than methods based on CT images or X-Rays because the usage ionizing radiation is avoided.

In literature different regression methods have been developed, that are based on diverse anthropometric measurements. The most populare are Bell et al. [16], Harrington et al. [4] and Seidel et al [17]. Bell et al. estimate the position of HJC as a constant percentage of the pelvic width (i.e. the distance between the position of the two anterior-superior iliac crests). Instead, Siedel et al. demonstrated that HJC position is a function not only of pelvic width but also of pelvic depth (distance between mid point of ASIS and mid point of PSIS)and pelvic height (distance between pubic symphysis and inter ASIS line). The anthropometric measurements used are pelvic width (PW), pelvc depth (PD) and clinical leg length (LL). Harrington et al. regression equation are written below (equation in mm):

$$\hat{x} = -0.24PD - 9.9$$

$$\hat{y} = -16PW - 0.04LL - 7.1$$

$$\hat{z} = 0.28PD + 0.16PW + 7.9$$

Harrington et al. method is the one that proved to perform the best within predictive methods according to [5]. The error the anterior-posterior direction (x) has a maximum value of 11.5mm and RMS is 5.88mm. For up-down direction (y) the maximum is 6.96mm with RMS of 3.65mm. Finally for medial-lateral direction (z) the maximum

value is 12 and RMS is 4.32mm. Harrington tested its algorithm on healthy adult and children as well as on children with spastic diplegic cerebral palsy, and it proved to provide an accurate HJC localization also in pathologic subjects.

2.4   Functional methods for HJC localization

Functional methods define the HJC from the relative movement between the femur and pelvis in a predefined reference system; HJC position is computed through a kinematic approach. Differently from predictive methods, the subject is asked to perform stan-
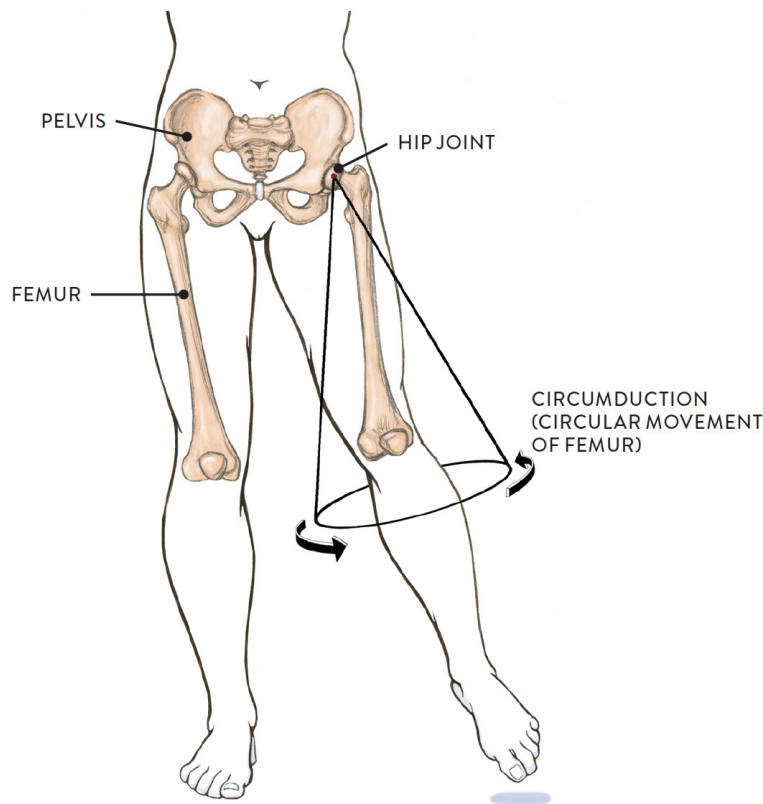
Figure 2.8: One possible relative movement of pelvis and femur.

dard movements, while an optical acquisition system measures the pose of the lower limb in the sensor reference frame. Each functional method has a standard acquisition

protocol for markers placement and motion pattern the subject is asked to perform. The data acquired are then processed in order to obtain a reliable estimation of HJC and each functional algorithm is characterized by it's own data processing strategy. The instrumentation used for the acquisition of the poses of the limb changes according to the application area. In motion analysis field, the pose is obtained by applying a cluster of markers on the limb surface. This procedure is completely non-invasive.

In CAOS techniques, instead, the markers are rigidly constrained to the underlying bones using proper instrumentation for orthopaedic surgical navigation procedures. The surgical tool are similar to that in Fig. 2.5) and each of them identifies a DRF. The set up for gait analysis produces results with lower accuracy than in CAOS. This is due to the fact that the first experimental set up is affected by a te presence of movement artifacts due to the presence of soft tissues and muscle at the interface between marker and bone surface.
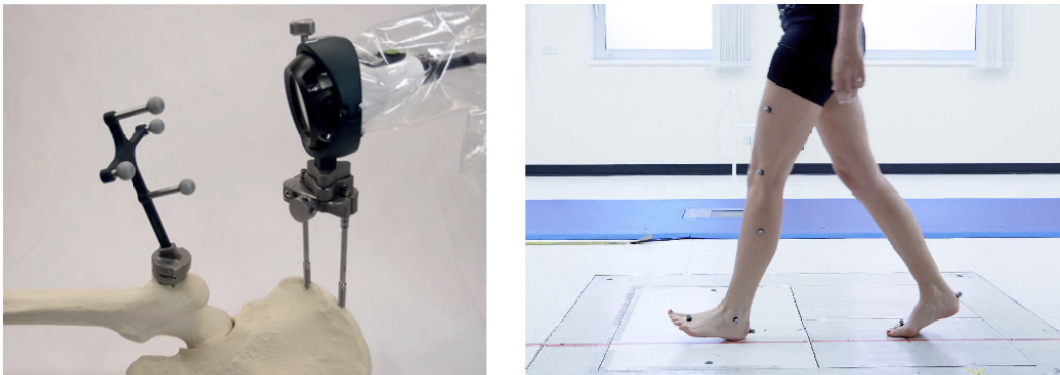
Figure 2.9: On the left example of marker placement for surgery, on the right example of marker placement for gait analysis

Functional methods for HJC localization can be divided into two main categories transformation techniques and sphere fitting techniques. In sphere fitting approach, through the elaboration of a dataset of femoral poses and under the hypothesis of an ideal stationary spherical joint, the centre of rotation (HJC) or the axis of rotation

of the articular joint is estimated. This algorithms have been implemented for motion analysis applications and therefore the data used are usually from skin markers. Several iterative techniques with least squares approach are presented in the literature. Some methods impose geometric constraints on the marker configuration [18], while other methods assume that each marker moves independently on a sphere centered in HJC.

Transformation techniques are characterized by the identification of local reference frame (RF) on each body segment of interest (femur and pelvis) and by transformations between RFs report the poses acquired in a common SDR. In 2015 Kainz et al. [6] made a wide review evaluating the performance of five sphere fitting methods (algebraic sphere fit ASF method, bias compensated bcASF, geometric sphere fit method GSF, and incomplete algebraic sphere fit method iAFS) and seven transformation techniques (centre transformation technique CTT, Holzreiter approach HR, helical pivot technique HPT, minimal amplitude point MAP, Monte Carlo pivoting MCP, revised functional method RFM, symmetric centre of rotation estimation SCoRE and Schwartz transformation technique STT). They concluded that, according to in vivo studies, the GSF method is the most accurate approach with an average error of 11 to 21 mm.

At NEARLab we performed a simulation of HJC localization by mean of sphere fitting on a phantom. We used Polaris VICRA®sytem for the acquisition procedure. The phantom used is composed by two bony segments made of rigid foam that represent the pelvis and the femur. The two segment are joined together with an elastic component that permit relative movements of pelvis and femur. In the preparatory phase we rigidly linked one surgical tool for pose acquisition on the pelvis (which identifies DRF_p)and another one on the distal femur (DRF_f). In the acquisition phase two passive maneuvers were performed on the femur segment. The acquired data are, expressed in DRF_p, are shown in Fig.2.10. The real HJC have been computed in Section 2.2 and resulted in position -80.5mm -13.1mm -88.0mm (x,y,z direction respectively). We applied least square sphere fitting algorithm on the data from femur DRF_f we obtained the following position for HJC position for the two maneuver. Maneuver 1: -81.01mm, -12.79mm,
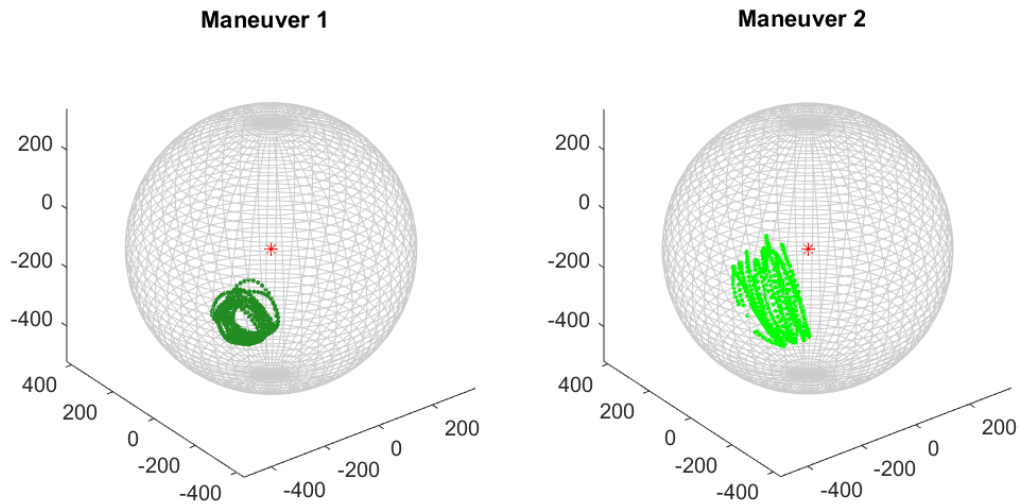
Figure 2.10: Plot of the acquired data from two different passive maneuver

-86.96mm (x,y,z direction respectively). Maneuver 2: -79.95mm, -13.45mm, -88.97mm (x,y,z direction respectively). The mean value of the two maneuvers is: -80.48 -13.12 -87.96 which corresponds to an error lower than 1mm for all the directions. The error is very low compared to the one in literature mentioned above. This is mainly due to the absence of movements artifacts which are estimated to be the main error source when computing HJC by means of functional methods [5].

2.5 Background on artificial neural networks

The artificial neural network (ANN), is a machine learning technique evolved from the idea of simulating biological neural network [19]. If our aim is to model a complex nonlinear system traditional regression methods may not be able to find relationships between input and outputs. Instead, due to their structure, ANN are intrinsically capable to

model nonlinear data, moreover binary input can be used together with continuous one. We exploited this capabilities of ANN to include gender among input parameters. Three critical elements define a neural network: node characteristics, network topologies and learning rule. The biological structure corresponding to the nodes are the neurons. The node, which basic model is shown in 2.11, receives n weighted input and sum them. The summation results of the inputs to one node is processed with the so called activation function that usually is a step function or a sigmoid. The output of the node is then given as input to the following hidden layer or to the output layer. Generally more
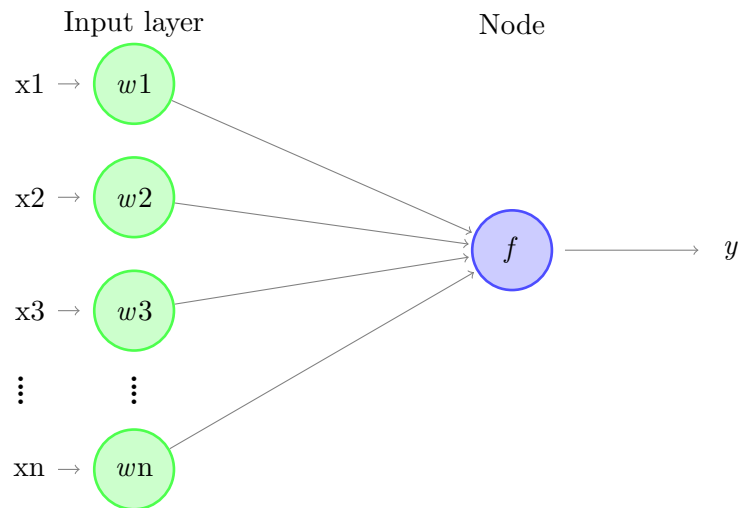
Figure 2.11: Model of one node of an artificial neural network.

nodes are aggregated into layers which are interconnected. The number of layer, the number of nodes in each layer and the way nodes are interconnected define the topology of a network.

Nodes can be connected in two ways one is forward connection with no loop back. In connection with loop back instead the output of the nodes can be the input to previous or same level nodes [19]. On this basis we can distinguish between feedforward networks and recurrent networks. In feedforward networks the signal goes one from input to output without going back and for this reason to each input corresponds a single output. On the contrary recurrent networks is dynamic; that is for one input the ANN produces

a series of outputs depending on the previous inputs and outputs values.

Learning algorithms determine how the weights are initialized and adjusted [19]. There are two main categories of learning rules: supervised learning and unsupervised learning. In supervised learning the weights are modified in order to minimize the error between the ANN output and the correct output. Of course a set of input with the corresponding output must be used for the train since the true output must be known. When the network produces the desired outputs for a series of inputs, the weights are fixed and the network can be put in operation. On the contrary, unsupervised learning is used when true output values are unknown. In this case network tries to find a trend in the input data on its own.

3

Dataset and model construction

In this chapter, we present material and methods used for the implementation of the neural network model for functional HJC estimation. In Section 3.1 the characteristics of the used datasets are shown. Then, in Section 3.3 we provide a description of the methods used for estimating HJC position with full input parameters. The effects of age and gender on the HJC localization are investigated in Sections 3.5 and 3.6. Finally, in Section 3.8, the effect of fat and skin artefacts is simulated and the performance of the estimation algorithm is analysed.

All the implementations and tests described in this chapter have been developed within MATLAB®environment.

3.1 Available dataset

The experimental data used to develop this thesis project came from three datasets collected from three different research group. Before getting into the details of the mentioned datasets, we want to introduce the anthropometric measurements we are going to use for HJC estimation. Please refer to Fig. 3.1 for a visual interpretation of the following parameters.

- *Leg Length (LL)*. Clinical leg length, measured from ASIS to medial epicondyle (ME) of the knee, then to medial malleolus (MM)

- *Pelvis Depth (PD)*. Distance between the left and right ASIS

- *Pelvis Width (PW)*. Distance between the ASIS midpoint and the PSIS midpoint
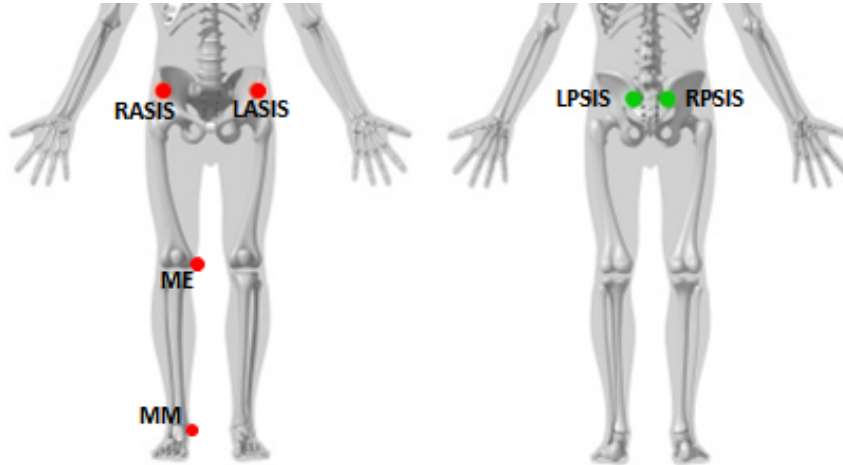
Figure 3.1: introduced by Hara et al. in [7] and utilized in this thesis.

The strong relationship between PD, PW and the position of HJC in a pelvis embedded coordinate system had already been observed by Seidel et al.[17], but they used pelvis height (i.e. perpendicular from pubic symphysis to inter ASIS line) to predict HJCz coordinate. In this work, as well as in [4], pelvis height is not included in the parameters because the palpation of pubic symphysis is not practical in routine clinical procedures. LL, PD and PW can be measured after locating 6 anatomical landmarks: left and right anterior superior iliac spine (ASIS), left and right posterior superior iliac spine (PSIS), right medial epicondyle of femur (ME) and right medial malleolus (MM). To evaluate the effectiveness of the HJC estimation, real hip joint centre was also identified. Differently from Harrington's work, together with the anthropometric measurements we introduced also gender and age as input parameters.

Dataset1 is the biggest one and data were acquired by R. Hara et al. in [7].

Due to its dimension, it is the one on which the neural networks are going to be trained. R. Hara et al. obtained tridimensional images of the bodies of 157 deceased individuals using computed tomography. Exactly 120 out of the 157 bodies correspond to adult individuals. They can be divided into 60 males and 60 females, each group presenting almost the same average age. The remaining 33 data belong to young individuals, more precisely to 24 male and 13 females, with the female group showing a higher average age. As expected, for the adult group, women tends to be shorter and lighter than men. In the children group, instead, the age difference leads to taller females. Informations on ethnic descent is not included in the dataset, but the authors state that all the subjects were Australian citizens. Data are resumed in Tab. 3.1. Hara et al. identified the anatomical landmarks by visual inspection of the 3D models obtained using CT scan, so their data are not affected by the presence of fat or skin artefacts. CT images were taken every 1.0 mm with a slice thickness of 1.5 mm in all planes. The coordinates of HJC are expressed in a pelvis embedded reference system. Pelvis' origin is set to the mid-point between the left and right ASIS with the y-axes pointing to right ASIS. The x-axes is set to be the transverse plane of the pelvis that contains both ASIS and the mid point of the two PSIS. See Fig.3.2
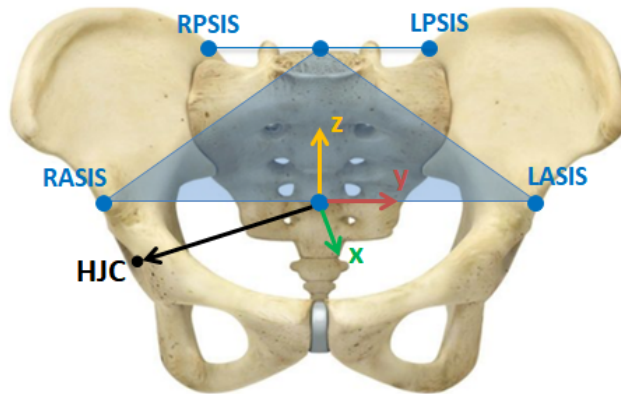
Figure 3.2: Pelvis embedded coordinates system for Dataset1 and the one used for the thesis project

- X is antero-posterior position of the hip joint centre

- Y is lateral-medial position of the hip joint centre

- Z is up-down position of the hip joint centre

Dataset2 is from Harrington et al. [4], it contains data from 32 subjects: 8 adults, 14 healthy children, and 10 children with spastic diplegic cerebral palsy. MRI scans of the pelvis were acquired using a 2.5mm slice width T1-weighted, three-dimensional sequence to optimise bone and muscle definition, with a gradient echo (TE/TR 20/ 15 ms) to maximise the speed of acquisition. A two-dimensional volume spin-echo sequence was also collected to aid orientation within the former images. The leg lengths of each subject were measured manually. All the patients were English citizens. In this case the pelvis embedded coordinate system for HJC position is the one shown in Fig. 3.3.
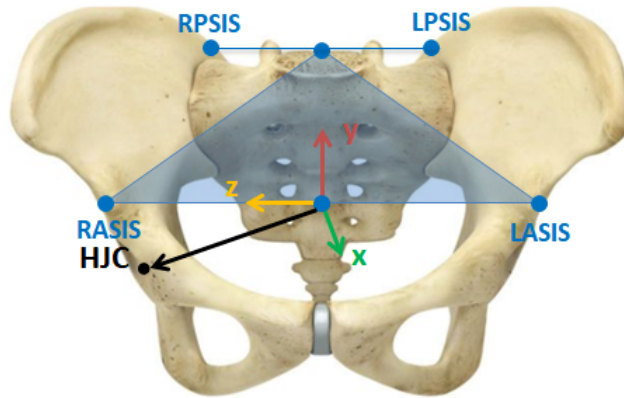
Figure 3.3: Pelvis embedded coordinates system for Dataset2 and Dataset3.

- X is antero-posterior position of the hip joint centre

- Y is up-down position of the hip joint centre

- Z is lateral-medial position of the hip joint centre

Dataset3 is from Leardini et al. [8], it contains data from 11 male adult subjects. The real position of the HJC was obtained using Roentgen stereophotogrammetric analysis (RSA). Four spherical 0.8 mm diameter tantalum balls were placed on the skin to obtain ASIS and PSIS anatomical landmarks. Some uncertainty affects LL measurements. In fact, LL is defined as the distance between ASIS and homolateral MM, but it is not mentioned whether the measurement is done by passing from ME or not. Also in this case the coordinate reference system is the one shown in 3.3. In the Tab. 3.1 the mean value of the used parameters are listed for each dataset and divided according to gender and adult/children differences.

Male adults									
	Number of sample	Age	Weigth	PW	LL	PD	HJCx	HJCy	HJCz
Dataset1	60	24.62	76.47	225.51	901.76	143.09	-44.79	84.48	-80.00
Dataset2	5	30.20	76.80	257.16	964	156.28	-45.32	92.54	-88.32
Dataset3	11	29.27	76.45	234.55	928.18	168.18	-51.37	88.19	-89.90
Mean		25.66	76.49	228.90	909.68	147.59	-45.78	85.55	-81.98
Female adults									
	Number of sample	Age	Weigth	PW	LL	PD	HJCx	HJCy	HJCz
Dataset1	60	25.12	66.73	217.51	844.76	142.15	-45.22	84.55	-76.71
Dataset2	3	27.00	59.67	225.13	865.00	144.63	-44.03	88.77	-82.90
Mean		25.21	66.40	217.87	845.72	142.26	-45.16	84.75	-77.00

Table 3.1: Mean value for the categories age, weight, PW, LL PD, HJCx, HJCy and HJCz for adult's data of all the dataset used in this thesis.

Male children									
	Number of sample	Age	Weigth	PW	LL	PD	HJCx	HJCy	HJCz
Dataset1	24	6.75	30.00	166.52	605.32	87.23	-25.37	58.84	-56.24
Dataset2 healthy	7	8.29	29.09	184.10	690.43	99.51	-32.44	64.23	-64.70
Dataset2 with cerebral palsy	5	9.8	30	170.44	675	99.74	-35.7	64.24	-61.58
Mean		8.28	29.48	173.69	656.92	95.49	-31.17	62.44	-60.84
Female children									
	Number of seample	Age	Weigth	PW	LL	PD	HJCx	HJCy	HJCz
Dataset1	13	8.85	37.77	177.45	680.64	97.25	-32.12	62.38	-60.68
Dataset2 healthy	7	8.43	29.36	178.16	711.21	106.60	-35.34	63.84	-68.04
Dataset2 with cerebral palsy	5	9.2	27.9	173.36	687	97.72	-35.46	65.78	-63.46
Mean		8.83	31.68	176.32	692.95	100.52	-34.31	64.00	-64.06

Table 3.2: Mean value for the categories age, weight, PW, LL, PD, HJCx, HJCy and HJCz for children's data of all the dataset used in this thesis.

3.2 Partitioning of data for ANN implementation and testing

The data used for the neural networks training and validation are a subset of the data in Dataset1. The 157 data in Dataset1 were randomly sorted and then divided so to have 100 data for training, 25 validation and 32 for testing, as showed in Fig. 3.4. The reason why we selected such a division is twofold; firstly, it is known that neural networks require a considerable amount of samples to be properly trained; secondly, we would like to obtain a dataset with the same cardinality as Harrington's. This will turn out to be convenient for our subsequent statistical test analysis, because it helps to avoid misclassification due to different sample size, as reported in [20]. Once
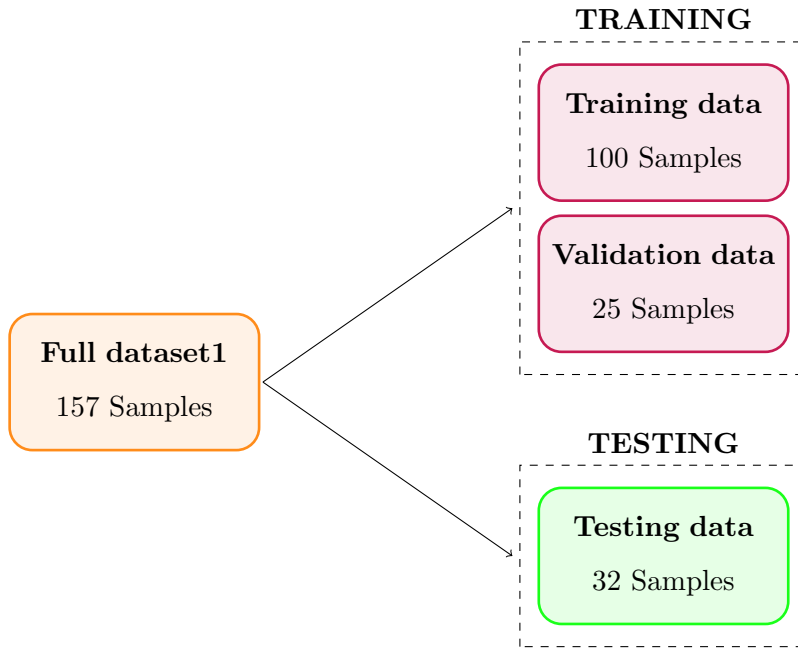
Figure 3.4: Scheme of dataset partition.

each network was trained we used two set of sample to test its behaviour and compare the localization error with the one obtained using Harrington's algorithm. To make an accurate comparison we evaluate the performance of the two method on the same dataset with which they have been developed and then on another dataset obtained merging the remaining datasets. The first test is made to evaluate the accuracy of the developed model compared to Harrington's and is made with 32 sample datasets; we will refer to this testing phase as accuracy test. The latter, instead is made to evaluate the accuracy of the algorithm when generalizing to other datasets, the used datasets had 43 samples coming form two different datasets that have been merged. We will refer to this testing phase as generalization test. For Harrington's algorithm the data came from the 32 samples of Dataset1 used for testing ANN performance and Dataset3. For our model the data came from Dataset2 and Daaset3. In Fig 3.5 the testing procedure is schematized.
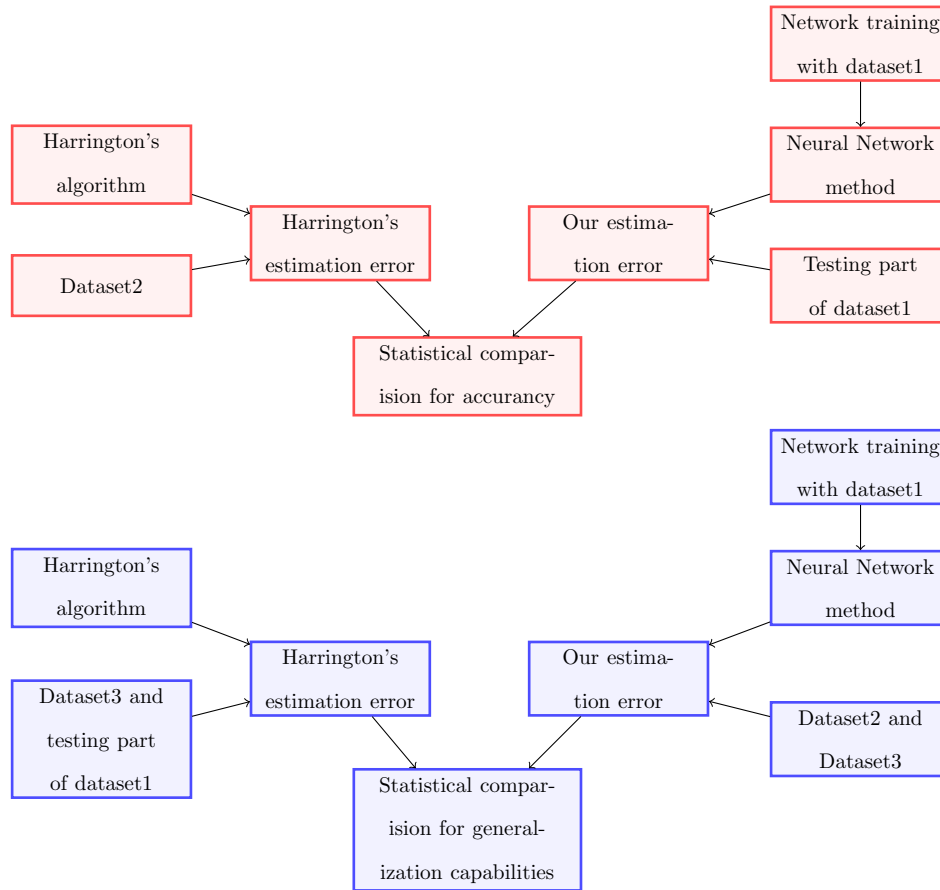
Figure 3.5: In red, test to compare accuracy of the two methods; in blue, test to compare accuracy of the network while generalizing to other datasets.

3.3 Models with full input parameters

As explained in section 2.5 there are three critical elements to define a neural network: number of nodes, network topologies and learning rule. In the following part of the chapter, we are going to explain in detail how we defined such elements to build the neural network.

Our goal is to find the coordinates of HJC from a pool of input parameter. Therefore, while different input parameter, number of output, hidden layer and nodes were used to train the ANN the purpose of the network remains the same: fitting the data. For

this reason the topology of the neural network must be feedforward to assure one single output for each set of inputs.

3.3.1 Estimation of HJCx HJCy and HJCz

The first network we implemented is the one that takes gender, age, PD, PW and LL as inputs, and returns the coordinates hip joint center, HJCx, HJCy and HJCz. This 5-inputs and 3-outputs network is represented in Fig.3.6. The activation function f
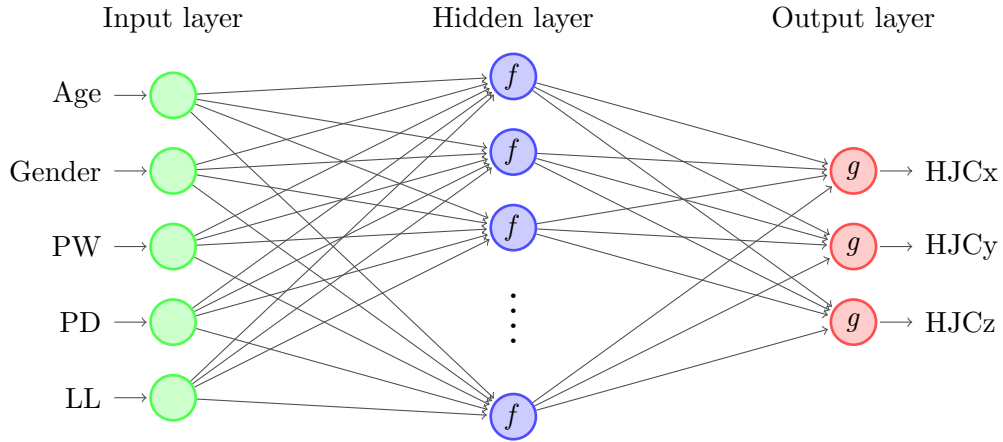
Figure 3.6: 5-input 3-output network

in the hidden layer is the sigmoid function, instead g is a linear function. Plenty of networks were implemented with different number of nodes (1 to 200) in the hidden layer and also with one to five hidden layers.We proceed by comparing the HJC estimation errors provided by these neural networks with different configurations among them. The outcome of this comparative process, which results are resumed in Tab. 3.3, suggested that the best performance is reached by networks with a number of nodes higher than 10 and with a single hidden layer. The presence of more than one hidden layer lead to an error that is three times the error with only one hidden layer. One hidden layer networks have very good performance also with only 2 nodes in the hidden layer and kept increasing their accuracy until 10 nodes in the hidden layer. For higher

number of nodes the neural networks kept performing good but with training time that was exponentially increasing. For this reasons, we selected for our analysis a 10-nodes one-hidden-layer network. The next step would be to select a suitable learning rule, as well as define the weight and bias initialization to train our network. Weights and bias were initialized with random values between -1 and 1. To assure best performances of the ANN we tried a few supervised learning algorithms: Levenberg-Marquardt, resilient backpropagation and Bayesian regularization algorithm. All the afore mentioned learning rules were tested on all the network trained and in all cases the best performance were assured by Bayesian regularization algorithm. Bayesian regularization is a mathematical process that converts a nonlinear regression into a "well-posed" statistical problem in the manner of a ridge regression [21]. The main drawback of this method is the increased training time which is almost three times higher than resilient backpropagation and twice Levenberg-Marquardt. This was not a problem in our case since the maximum obtained was about 3h (one hidden layer with 500 nodes), and this is a reasonable time for training. Moreover once the network is trained it takes a few ms to get the estimation of HJC position given the input parameters. In tab 3.3 are reported the results of some of the implemented networks tested on the testing subset of Dataset1. All ANN in Tab. 3.3 were used also to estimate HJC of sample from Datase2 and Dataset3. In the Tab.3.4 the results are summarized. In the following chapter we will refer to this algorithm with the name *Algorithm 1*.

3.3.2   Estimation of HJCx HJCy and HJCz independently

As we have seen in the results of the networks implemented in Section 3.3 there isn't the same accuracy in the estimation of all three coordinates of the HJC, so we decided to develop three distinguished networks each able to deduce one of the coordinates of the joint centre (HJCx, HJCy and HJCz). For all the networks the input were the same as shown in Fig.3.7. Again different network were implemented but the best performance were assured with 1-hidden layer 10-nodes network with and as training

28

Hidden layer and nodes	HJCx	HJCy	HJCz	Distance
200	3.23	3.12	2.69	5.97
100	3.21	3.22	2.68	6.00
2	3.62	3.30	3.04	6.48
10	3.30	3.01	2.67	5.95
[10 10 10]	8.13	6.23	11.10	16.73
[5 5 5 5 5]	5.40	4.84	6.32	10.99
Harrington algorithm on the same data for testing	4.94	2.89	3.47	7.51

Table 3.3: In the first column there is represented the number of hidden layer (number of numerical elements) and the number of nodes in each hidden layer. In the column HJCx HJCy and HJCz is reported the mean of error's absolute value. In column distance the mean of the distances is reported.

	HJCx error			HJCy error			HJCz error			Distance		
	Mean	RMS	Max	Mean	RMS	Max	Mean	RMS	Max	Mean	Variance	RMS
NN accuracy	3.31	4.06	10.17	3.08	3.92	10.10	2.77	3.27	7.49	6.01	2.58	6.52
H accuracy	4.94	5.88	11.50	2.89	3.65	6.96	3.47	4.32	12.00	7.51	3.23	8.16
NN generalization	5.15	6.27	13.27	3.75	4.86	12.19	5.17	6.84	21.25	9.39	4.70	10.48
H generalization	5.45	6.98	15.44	5.08	6.12	13.22	6.19	8.20	22.02	11.18	5.41	12.39

Table 3.4: Results of *Algorithm 1*. Mean of HJC errors are the mean of the absolute value of the errors, RMS is the root mean square of the error and Max is the maximum error encountered without sign.

function Bayesian regularization, therefore, only the results of these networks are shown. In Tab. 3.5 the statistics on the error in the estimation of HJC using these networks are summarized and it is possible to see how close they are to the one obtained in the previous section. In the following chapters we will refer to this algorithm as *Algorithm 2.*
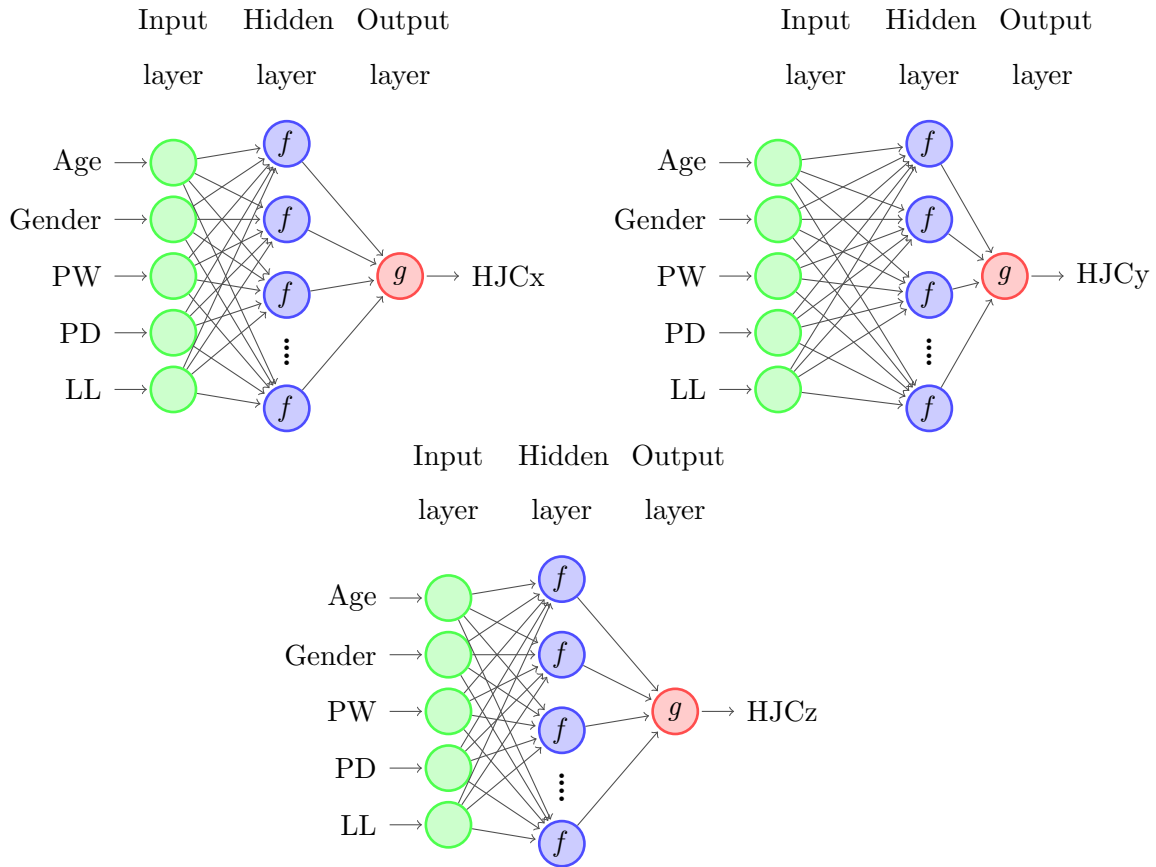
Figure 3.7: Three network trained independently each one with 5 input and 1 output.

3.4 Network with HJCy as input to estimate HJCx and HJCz

Both the algorithm implemented in chapter 3.3 proved to be able to estimate HJCy in a very accurate way (considering RMS value), on the contrary estimation of HJCx and HJCz had considerably higher RMS error when generalizing to other datasets. Therefore, in this section we tried to find a solution to decrease also the HJCx and HJCz estimation. To do so we decided to start from the estimation of HJCy, and then use this estimation as an input parameter of the neural networks for the estimation of HJCx and HJCz.

	HJCx error			HJCy error			HJCz error			Distance		
	Mean	RMS	Max	Mean	RMS	Max	Mean	RMS	Max	Mean	Variance	RMS
NN accuracy	3.30	3.79	7.29	3.21	4.07	10.68	2.81	3.52	9.62	6.05	2.62	6.58
H accuracy	4.94	5.88	11.50	2.89	3.65	6.96	3.47	4.32	12.00	7.51	3.23	8.16
NN generalization	5.13	6.15	12.18	4.02	5.11	12.82	4.99	6.51	19.48	9.34	4.41	10.31
H generalization	5.45	6.98	15.44	5.08	6.12	13.22	6.19	8.20	22.02	11.18	5.41	12.39

Table 3.5: Results of *Algorithm 2*. Mean of HJC errors are the mean of the absolute value of the errors, RMS is the root mean square of the error and Max is the maximum error encountered without sign.

Figure 3.8: Network for estimation of HJCy is developed independently, the networks for HJCx and HJCz are made using the output of the HJCy estimation ANN as an input parameter.

As it can be seen in Fig. 3.8 the ANN implemented for HJCy is made up in the same way as in the previous section (5-inputs, 1-output). The networks for HJCx and HJCz

31

estimation instead have 6 input parameters and one output parameter each. The results obtained with this ANN fashion lead a decrease in the overall distance between estimated HJC and true HJC. The best neural networks for HJCx and HJCz localization have 15 nodes grouped into one hidden layer. The increase of nodes number may be due to the augmented number of input parameters. Learning algorithm is Bayesian regularization with weight initialized with random numbers in range [-1, 1]. f is the sigmoid function while g is a linear function. Although the networks showed here may seem to perform the same as the two in Section 3.3, with further analysis in the Chapter 4.1 will be proved using statistical hypotesis test that the neural networks here developed are the networks that give the lowest distances between real and estimated HJC. In the following chapter we will refer to this algorithm with the name *Algorithm 3*.

	HJCx error			HJCy error			HJCz error			Distance		
	Mean	RMS	Max	Mean	RMS	Max	Mean	RMS	Max	Mean	Variance	RMS
NN accuracy	3.11	3.59	7.52	3.21	4.11	9.76	2.78	3.45	9.27	5.94	2.58	6.46
H accuracy	4.94	5.88	11.50	2.89	3.65	6.96	3.47	4.32	12.00	7.51	3.23	8.16
NN generalization	5.31	6.34	12.35	3.80	4.77	11.66	4.98	6.49	19.24	9.26	4.44	10.25
H generalization	5.45	6.98	15.44	5.08	6.12	13.22	6.19	8.20	22.02	11.18	5.41	12.39

Table 3.6: Results of *Algorithm 3*. Mean of HJC errors are the mean of the absolute value of the errors, RMS is the root mean square of the error and Max is the maximum error encountered without sign.

3.5   Input gender free network

Male and female differences in pelvis shape is well known and it is considered to be linked intimately with its adaptive functions; pelvis shape represents the total response to the requirements for efficient bipedalism and parturition. In particular the female pelvis has evolved to its maximum width for childbirth and the male pelvis has been optimized for bipedal locomotion. [22][23]. The structure of the pelvis is significantly
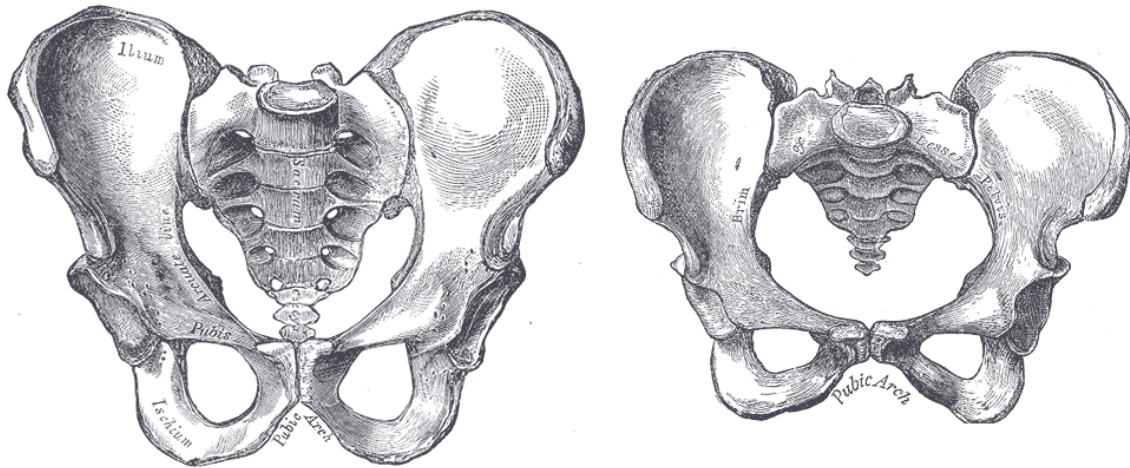
Figure 3.9: Differences between male (left) and female (right) pelvic bone shape.

heavier and thicker in male than in female and within the variations due to sexual dimorphism there is the overall shape which it has been demonstrated to have a more rounded frame in the female pelvis [23]. The main differences between man and woman pelvic bone is that females have: iliac bones more flared, angle of pubic arch grater, higher distance between ischial spine and sacral curvature shorter and wider. The pelvic inlet is said to be oval-shaped in female and heart-shaped in males Fig. 3.9. Finally the male acetabulum has been designed to fit a bigger femur head.

The ANN developed for testing the importance of including gender as parameter for HJC localization estimation was developed using a fashion very similar to the one in section 3.4 with estimation of HJCy that is then used as input parameter for HJCx and HJCz computation. The best performing network had one hidden layer with 10 nodes, learning algorithm was Bayesian regularization with all weights initialized with random numbers in range [-1, 1]. f is a sigmoind function and g a linear one. A graphic rapresentation of the network is shown in Fig. 3.10. In Tab. 3.7 the results obtained with the network are summarized. It is possible to see that the accuracy of the network on the dataset it was trained on keeps almost the same with RMS value of 3.90mm(previously 3.59mm), 4.09mm (previously 3.76mm) and 3.52mm (previously
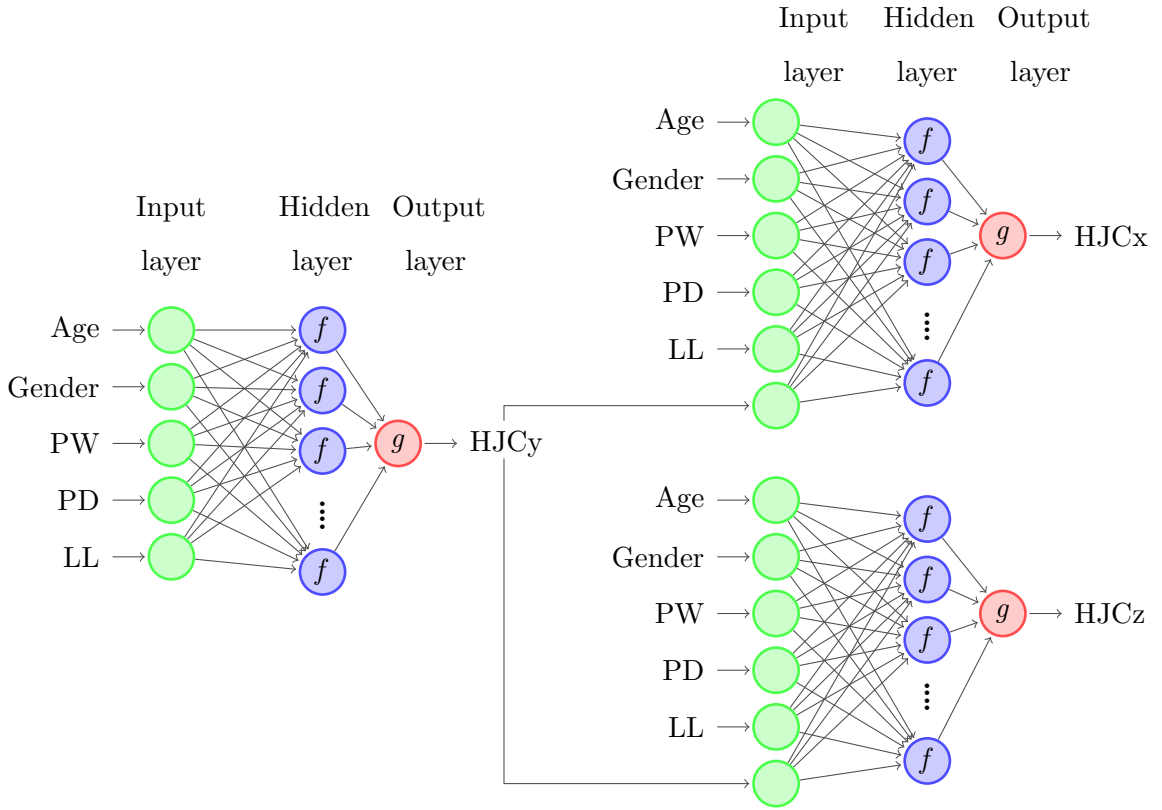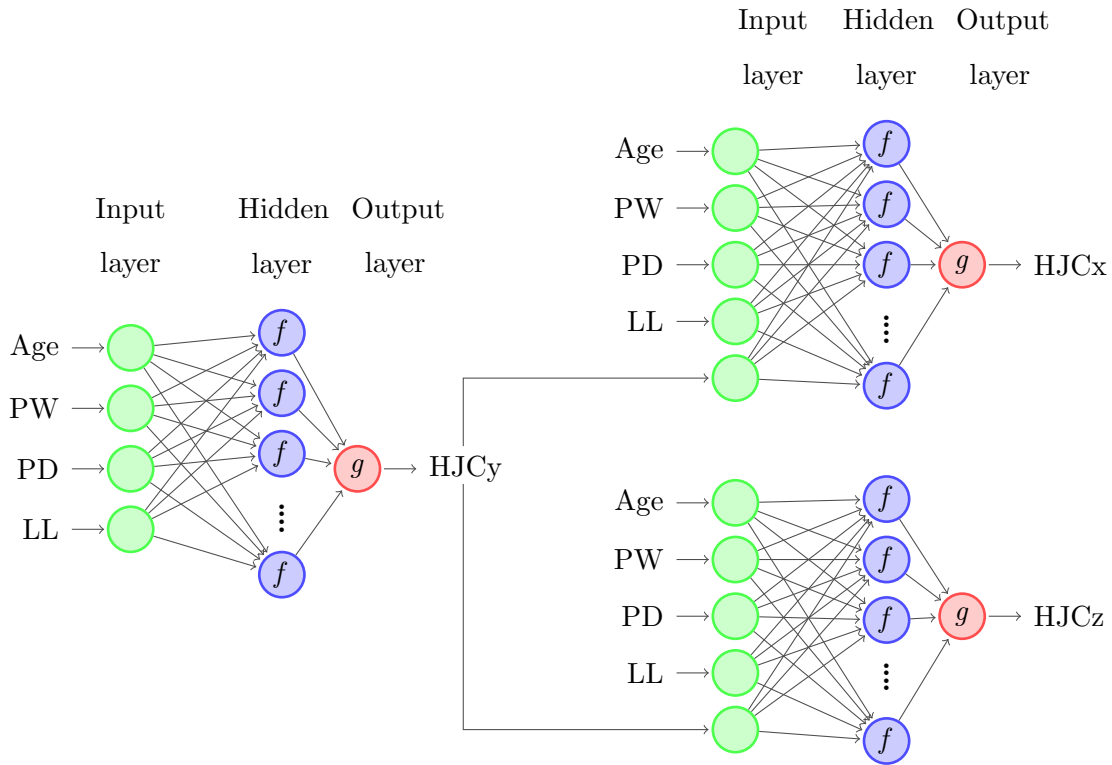
Figure 3.10: Network for estimation of HJCy is developed independently, the network for HJCx and HJCz is made using the output of the HJCy estimation ANN as an input parameter. In this case there isn't gender among the input parameters

3.45mm) for HJCx, HJCy and HJCz respectively. On the contrary there is a consistent worsening in the generalization capability of the network which is particularly clear having a look to the maximum HJCx error which goes from 12.35mm (network with gender) to 22.81mm which corresponds af an almost 50 % increase in localization error. More detailed statistical analysis comparing this network and the one in section 3.4 will be held in chapter 4.1. In the following chapter we will refer to this algorithm as *Algorithm 4.*

	HJCx error			HJCy error			HJCz error			Distance		
	Mean	RMS	Max	Mean	RMS	Max	Mean	RMS	Max	Mean	Variance	RMS
NN accuracy	3.36	3.90	8.43	3.31	4.09	10.30	2.84	3.52	9.53	6.12	2.67	6.66
H accuracy	4.94	5.88	11.50	2.89	3.65	6.96	3.47	4.32	12.00	7.51	3.23	8.16
NN generalization	7.06	9.27	23.81	3.92	4.94	12.17	5.03	6.68	20.52	10.76	6.32	12.44
H generalization	5.45	6.98	15.44	5.08	6.12	13.22	6.19	8.20	22.02	11.18	5.41	12.39

Table 3.7: Results of *Algorithm 4*. Mean of HJC errors are the mean of the absolute value of the errors, RMS is the root mean square of the error and Max is the maximum error encountered without sign.

3.6 Input age free network

Analysing our dataset it is possible to see that data from children are considerable different from adults one. This difference is surely due to the different stature and wight of the subjects. Another reason may be due to the fact that since they are not skeletally fully matured they may have a slightly different shape of pelvic bone compared to adult of the same gender. For this two reasons we included age as input parameter for the ANN in the first place.

In this section we aim at evaluate if age is actually improving the HJC estimation, to do so we implemented a new network with the same structure of the one in Fig. 3.10, with the only difference that the input parameter age is substituted by the gender. As it is possible to see analysing the results resumed in Tab. 3.8 the HJC estimation is almost the same as in section 3.4. Neural networks have the intrinsic capability of avoiding usage of non relevant input data, and this may be what happened with age parameter: the weight associated are very small and so the overall estimation in not very much affected when age is no longer used. More detailed analysis is carried out in Chapter 4. In the following chapter we will refer to this algorithm as *Algorithm 5*.

	HJCx error			HJCy error			HJCz error			Distance		
	Mean	RMS	Max	Mean	RMS	Max	Mean	RMS	Max	Mean	Variance	RMS
NN accuracy	3.13	3.67	7.31	3.40	4.57	10.33	2.85	3.61	9.83	6.22	3.00	6.88
H accuracy	4.94	5.88	11.50	2.89	3.65	6.96	3.47	4.32	12.00	7.51	3.23	8.16
NN generalization	5.34	6.40	12.49	3.82	5.07	12.80	5.02	6.50	18.87	9.37	4.64	10.44
H generalization	5.45	6.98	15.44	5.08	6.12	13.22	6.19	8.20	22.02	11.18	5.41	12.39

Table 3.8: Results of *Algorithm 5*. Mean of HJC errors are the mean of the absolute value of the errors, RMS is the root mean square of the error and Max is the maximum error encountered without sign.

3.7 Net trained with Harrington data

In order to evaluate more in detail if the capability of ANN methods are better than Harrington's linear regression we implemented some network also using Harrington dataset for the training. We tried using different combination of hidden layer (one to 5) and numbers of nodes (1 to 100) but the result we obtained was slightly worst than Harrington method itself. Since ANN proved, as showed in 3.4, to have very good lending in solving our fitting problem the lack of performance of this network may be due to the very little number of sample used for the training (only 32).

3.8 Fat and skin artefact simulation

After implementing neural networks using imaging data we decided to make the discussion more complete by simulating the presence of noise due to layers of skin muscle and fat between the anatomical landmarks located on the bones and the corresponding point identified by the cutaneous markers. To do so we added noise to the data from Dataset1 before training again the network; since we are now simulating the condition of markers placed on the skin another parameter starts to be relevant: body mass index

(BMI).

$$BMI = \frac{weight(kg)}{height^2} \frac{[kg]}{[m^2]}$$

The relationship between BMI index and the subcutaneous adipose tissue depth (SATD) has already been investigated leading to the conclusion that higher BMI index are consistent with bigger SATD [24]. In the implementation of our ANN we already had a parameter that is strongly related with subject height which is LL (50 % of total height) [25] but so far no input was accounting for weight so we decided to include it in this analysis. Two simulation of the error were performed that were equal except for the noise on PD. The error added to the parameter is summarized below:

- *Gender*: no error added

- *Age*: no error added

- *Weight*: no error added

- *Leg Length*: random error in the range ± 30mm

- *Pelvis Depth (without BMI)*: 10mm + random error in range 0mm-20mm

- *Pelvis Depth (with BMI)*:10mm + BMI and multiplied by a random error in range 0-1. Which correspond to an error in range 10mm-37.82mm

- *Pelvis Width*: random error in the range ± 10mm

The error on age and gender was set to 0 for obvious reasons. We didn't add noise to the weight because the measure was made with standard balance. The error on LL and PW were chosen according to [26] which states that mean error on marker placement in relaxed condition is about 10mm, since for LL measurement three markers need to be placed we set a error in range ± 30mm. For inter ASIS distance error is lower because we are not concerned about antero-posterior displacement of the marker and is of ± 5mm for each of the two markers 8total of ±10mm). For this statement we have assumed an equal thickness in the layer of skin, muscle and fat at the right and left

ASIS, and consequently the error in the antero-posterior direction, although present, does not influence the final value of the inter ASIS distance. According to [27] PD is
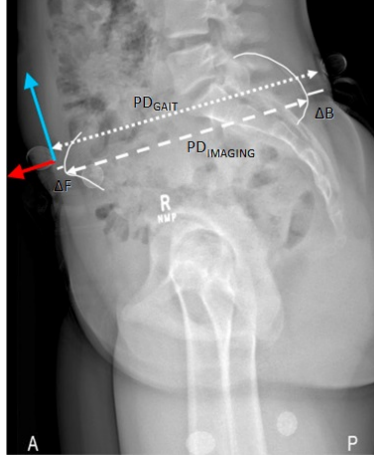
Figure 3.11: Difference between PD_{GAIT} and $PD_{IMAGING}$ on low dose bi-planar X-ray image[27]

the main source of error associated to predictive methods. It is important to note that soft tissue located between the ASIS and PSIS markers and the corresponding bony landmarks have a direct effect on PD as shown in Fig. 3.11. We can approximate this relationship by

$$PD_{GAIT} = PD_{IMAGING} + \Delta F + \Delta B$$

where PD_{GAIT} is the measure obtained from the ASIS and PSIS markers, $PD_{IMAGING}$ the measure obtained directly from the bony landmarks deduced from imaging data and ΔF, ΔB the thickness of the soft tissues between the bone and the skin at the front and the back of the pelvis respectively. There is no obvious equivalent relationship for PW and LL. While simulating the artefacts over PD we considered an always positive error which minimum value wa set to 10 mm. Then we have summed to the latter two different kind of random error. In the first case we used a random noise of $\pm$ 20mm which leads to an error bounded between 10mm and 30mm. In the second case we added a random noise in range [0,1] multiplied by BMI.The added error is bounded between 10mm and 40mm(which is consistent with [24]), and the actual maximum value

obtained in the simulation was 37.82mm.

Once the simulation of skin and fat artefact was performed we started implementing the ANN one this data. Again the dataset was divided so to have 100 random samples for training, 25 for validation and 32 for testing the network performances. Many fashion of the network were tested until finding the best performing which consiste in one hidden layer fully connected network as shown in Fig 3.12. As in previous network all weight were initialized with random numbers in range [-1, 1], the learning algorithm used is Bayesian Regularization, f is a sigmoid function and g is a linear function. As previously
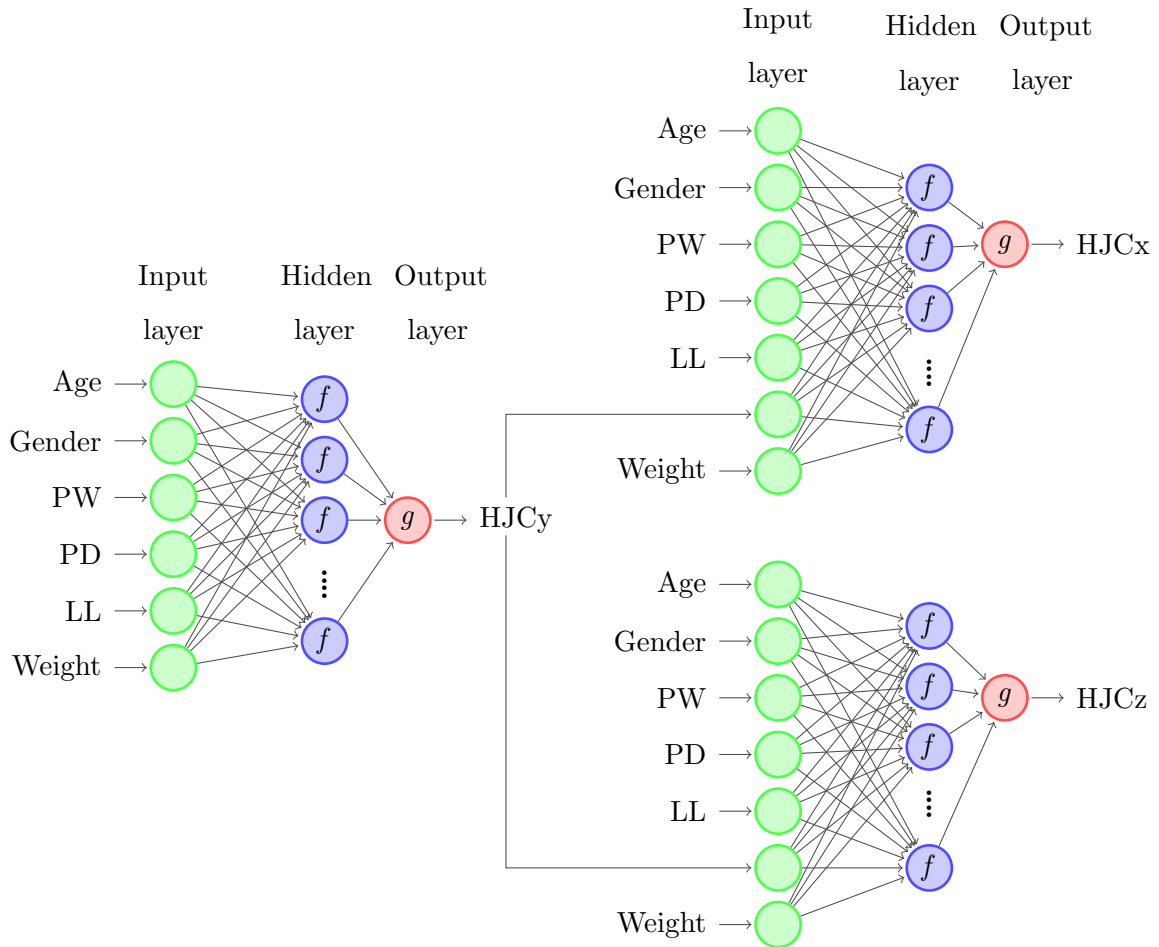
Figure 3.12: First HJCy is estimated, then HJCy is used as input parameter for HJCx and HJCz computing. Differently from 3.8 the weight was included as input parameter.

mentioned we trained the network with two different simulation of the PD skin artefact. When BMI was not used in the PD error simulation the best performing network had 15 nodes in the hidden layer for the estimation of all coordinates of HJC, the number of node increase to 20 when BMI was included in artifact simulation. If we look back to section 3.4 we can see that the optimum number of nodes for the networks with six input parameter is 15, in the case of no usage of BMI as error parameter the number is the same. This may be due to the fact that since skin and fat artefact over all the anthropometric parameters (LL, PD and PW) have no correlation with weight and also the PD, PW and LL are measured on the actual bony landmark, there is no correlation with weight in none of the date. Therefore including weight as input parameter is not leading to any improvement. On the contrary when BMI index is used for simulation of the error over PD the best networks have 20 nodes, and we have an overall increase of accuracy, compared to the white noise only. In the following chapter we will refer to the algorithm developed without BMI in artifact simulation with the name *Algorithm 6* and the one implemented including BMI in the simulation with the name *Algorithm 7*.

	HJCx error			HJCy error			HJCz error			Distance		
	Mean	RMS	Max	Mean	RMS	Max	Mean	RMS	Max	Mean	Variance	RMS
Algorithm 6	3.41	4.19	9.34	3.37	4.39	9.11	3.07	3.66	7.10	6.50	2.88	7.09
Algorithm 7	3.13	3.85	9.63	3.51	4.35	9.25	3.02	3.54	6.61	6.28	2.64	6.80
H without noise	4.94	5.88	11.50	2.89	3.65	6.96	3.47	4.32	12.00	7.51	3.23	12.39

Table 3.9: Results of *Algorithm 6* and *Algorithm 7*. Mean of HJC errors are the mean of the absolute value of the errors, RMS is the root mean square of the error and Max is the maximum error encountered without sign.

4

Results and discussion

In this chapter the statistical analysis on the results is carried out. In the first part we make a comparison, through statistical hypothesis tests, on the performance of the algorithm implemented in the previous chapter and Harrington's algorithm. In the second part we analyse, from a formal statistical point of view, the algorithm performance with and without gender and age as input parameter. The statistical hypothesis tests described in this chapter have been developed within MATLAB®environment.

4.1   Improvement in the field

In this section, we will perform the statistical analysis on the HJC estimation data we obtained by applying the algorithms developed in Chapter 3. The analysis is made through the comparison with Harrington's algorithm which, as mentioned in Section 2.4, is the best current predicting method, according to Fiorentino et al. [5] and Kainz et al. [6]. The comparison, made through statistical hypothesis tests, is going to be performed on the difference between the real data, obtained by imagining technique, and the data estimated by ANN and with Harrington's method. We will evaluate three separate parameters for x, y and z direction, and a parameter that involves the three

directions together. In particular, we consider the *squared HJCx,y,z error*, defined as follows:

$$squared\,HJCx,y,z\,error = \begin{cases} squared\,HJCx\,error \\ squared\,HJCy\,error \\ squared\,HJCz\,error \end{cases} = \begin{cases} (HJCx_{true} - HJCx_{est})^2 \\ (HJCy_{true} - HJCy_{est})^2 \\ (HJCz_{true} - HJCz_{est})^2 \end{cases}$$

(4.1)

and the *distance*, described below as

$$distance = ||HJC_{true} - HJC_{est}||,$$

(4.2)

where

$$HJC_{true} = \begin{bmatrix} HJCx_{true} \\ HJCy_{true} \\ HJCz_{true} \end{bmatrix} \quad \text{and} \quad HJC_{est} = \begin{bmatrix} HJCx_{est} \\ HJCy_{est} \\ HJCz_{est} \end{bmatrix},$$

(4.3)

and $|| \cdot ||$ is the Euclidean norm. In this way $||HJC_{true} - HJC_{est}||$ corresponds to the 3D distance between the true HJC and the estimated one. We are convinced that the introduction of this *distance* parameter in the statistical comparison is highly important, since it is the only parameter that gives an overall accuracy evaluation of the HJC estimate for each subject.

We now divide the statistical analysis in three parts. In Section 4.1.1 we will compare the data obtained applying our ANN on the dataset used for training the network (Dataset1), and Harrington's regression equation on its own dataset (Dataset2). In Section 4.1.2 the tests are performed on the data obtained by applying the aforementioned algorithms on other datasets. Fig. 4.1 shows a diagram resuming the performed tests. Finally, in Section 4.1.3 we will perform the statistical analysis on data with simulated noise addiction.
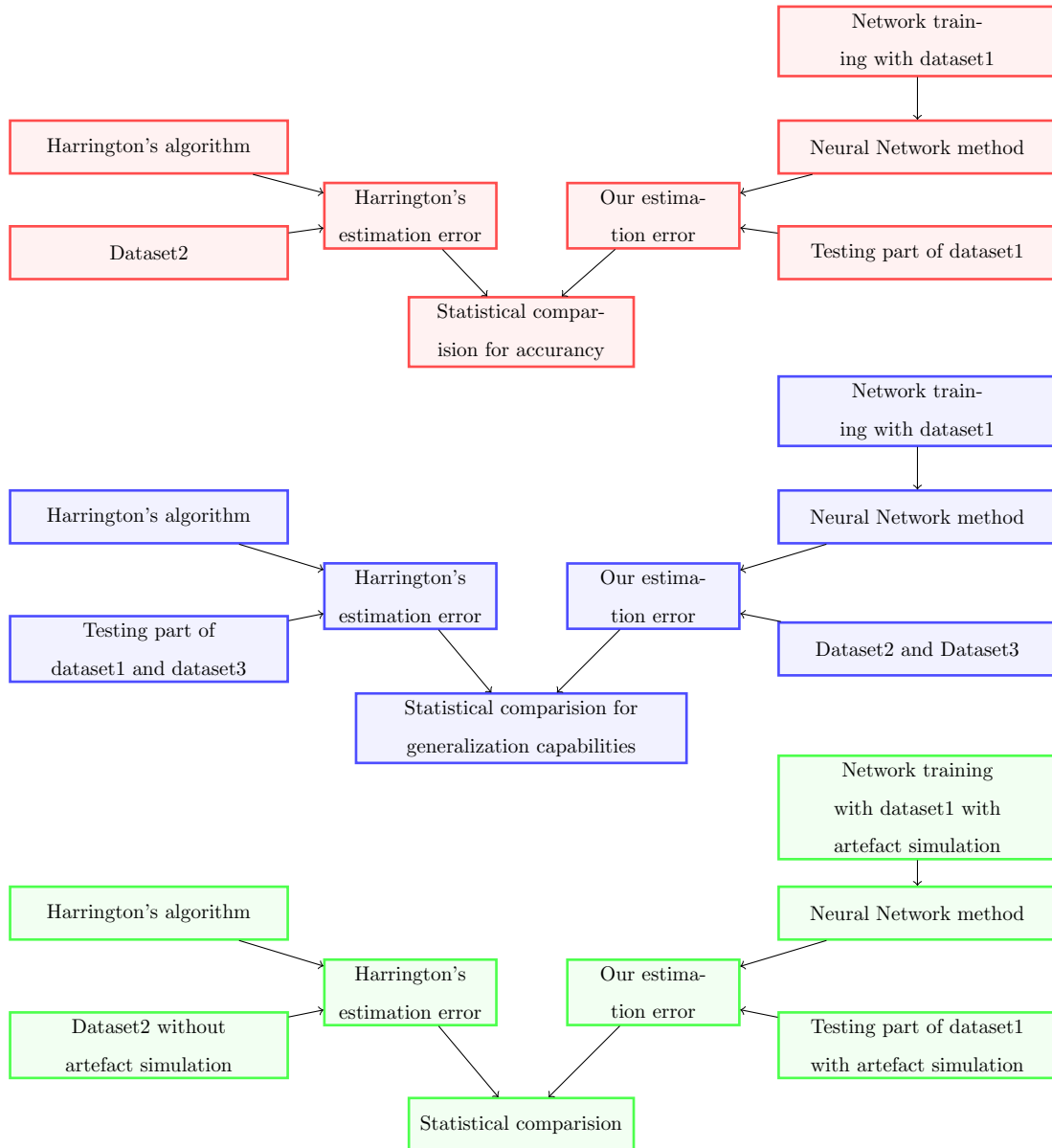
Figure 4.1: In red, test to compare accuracy of the two methods; in blue, test to compare accuracy while generalizing to other datasets; in green the statistical analysis of data with simulated fat and skin artefact.

4.1.1 Test on accuracy data

The data we will use here were obtained by applying the implemented algorithms on the testing subset of Dataset1. The gold standard data were obtained by applying

Harrington's algorithm on Dataset2.

Before performing the statistical comparison we evaluated whether the data under analysis are normally distributed or not. To do so, we performed two different tests: Lilliefors and Chi-squared test for normality. The tests were executed on the *squared HJCx,y,z error* and on the parameter *distance*; the results are resumed in Tab. 4.1.

NORMALITY TEST								
	Squared HJCx error		Squared HJCy error		Squared HJCz error		Distance	
	Lilliefors normality	Chi-squared normality	Lilliefors normality	Chi-squared normality	Lilliefors normality	Chi-squared normality	Lilliefors normality	Chi-squared normality
Algorithm 1	no	no	no	no	no	yes	yes	yes
Algorithm 2	no	yes	no	no	no	no	yes	yes
Algorithm 3	no	yes	no	no	no	no	yes	yes
Algorithm 4	no	yes	no	yes	no	no	no	yes
Algorithm 5	no	yes	no	yes	no	no	no	yes
Harrington	no	yes	no	yes	no	no	yes	yes

Table 4.1: Results of the normality test over *squared HJCx,y,z error*. In the first 5 rows the data are from our predictive method, in the last one data are from Harrington's.

As it is possible to see from the table the Lilliefors test is stricter than Chi-squared in the evaluation of normality. This is due to the fact that Lilliefors is a non-parametric test, while Chi-squared test is parametric. This analysis proved that the *squared HJCx,y,z error* in x, y and z direction is most of the time not normally distributed according to Chi-squared test, and never normally distributed according to Lilliefors test. Instead, the *distance* is always normally distributed, except when we apply the Lilliefors test to the network without gender (*Algorithm 4*) and without age (*Algorithm 5*).

Due to the results obtained about the normality of the distribution of the data, we decided to perform two different type of one-sided hypothesis test. For *squared HJCx,y,z error* data we performed a two-sample Kolmogorov-Smirnoff one-sided test, while for *distance* we did a one-tail two-sample t-test. Kolmogorov-Smirnoff test is a

non-parametric test that makes inferences about the equality of two probability distributions. It can be used to compare a sample distribution with a reference probability distribution, or to compare two samples between themselves, which is our case. For this test the null hypothesis (H0) to be rejected is that the two data came from the same distribution, while the alternative hypothesis (H1) is that the estimation error values obtained with Harrington method tend to be larger than those computed with ANN algorithm.

The two-sample t-test is usually employed to verify if the mean value of two normally distributed data samples are equal or not. In our case we performed the test with the null hypothesis (H0) of equal mean of two samples of the *distance* data, and the alternative hypothesis (H1) that the mean value of *distance* computed with Harrington's HJC estimation algorithm was higher than the mean value of *distance* computed with ANN-based estimation algorithm.

STATISTICAL COMPARISON				
	Distance t-test		**Distance K-S test**	
	Is better?	**p-value**	**Is better?**	**p-value**
Algorithm 1	yes	0.022	-	-
Algorithm 2	yes	0.026	-	-
Algorithm 3	yes	0.018	-	-
Algorithm 4	yes	0.032	yes	0.035
Algorithm 5	10%	0.051	yes	0.035

Table 4.2: Statistical hypothesis tests for the comparison of Harrington's method with ANN. On the distances we performed t-test, and for data non-normally distributed according to Lilliefors test, also a Kolmogorov-Smirnoff test

The results of Kolmogorov-Smirnoff test on *squared HJCx,y,z error* proved, at 5% significance level, that the *Algorithm 3* and *Algorithm 5* have improved HJCx estimation. Instead, for *Algorithms 1, 2* and *4*, there is statistical evidence of HJCx estimation improvement but only at 10% significance level. We found no proves of HJCy

and HJCz increase of accuracy. On *squared HJCy,z* we performed another Kolmogorov-Smirnoff test with the same null hypothesis as before but with the alternative hypothesis that the Harrington's samples have smaller error than ours. This last test never rejected H0 which means we don't have statistical evidence that Harrington's results have smaller errors than ours in y and z directions. According to the above consideration, we can state that the localization of HJC made with ANN have lead to an improvement in the estimation accuracy of the x-direction, while no improvement is shown in y and z directions. To make a comparison that takes into account the three direction x, y and z together, we analysed the *distance* between the real HJC and the estimated one (Tab. 4.2). Data in green are the one that proved to have lower error than Harrington's at 5% significance level, while in orange are reported the data that proved to have lower error than Harrington's but at 10% significance level. The Chi-squared test on *distance* data proved all the data to be normally distributed, so we used the two-sample one-sided t-test for the comparison. According to this test, there is statistical evidence that the *distance* between the real HJC and the one estimated with ANN is smaller with our algorithms than when estimation is made with Harrington's method. From this analysis we proved to have statistical evidence, at 5% significance level, that using ANN leads to an improvement of overall HJC estimation. Additionally, we executed the Kolmogorov-Smirnoff test on the data obtained with *Algorithms 5* and *6* since they were not normal according to Lilliefors test. The results of this last two tests is consistent with the one obtained before, assuring the statistical evidence of smaller HJC localization error.

The networks mentioned in this chapter proved to have lower mean value of *distance* than Harrington's. All of them allowed us to obtain an average *distance* between real and estimated HJC slightly above 6mm (except *Algorithm 3* slightly below 6mm). The mean value of *distance* obtained with *Algorithm 3* corresponds to an accuracy improvement of 21% with respect to Harrington's method. Furthermore there is a decrease of variance and RMS value of 20% each compared to Harrington's data.

4.1.2 Test on generalization data

The second test set evaluates the capability of the algorithm to generalize the results to other datasets. Therefore, we used the ANN (trained on Dataset1) to estimate the HJC from the data in Dataset2 and Dataset3. Harrington's algorithm was used to localize the HJC of the subjects in the testing subset of Dataset1 and in Dataset3. Again, before starting statistical comparison, we wanted to evaluate if the data were normally distributed. The results of the normality tests are resumed in Tab. 4.3.

	NORMALITY TEST							
	Squared HJCx error		Squared HJCy error		Squared HJCz error		Distance	
	Lilliefors normality	Chi-squared normality	Lilliefors normality	Chi-squared normality	Lilliefors normality	Chi-squared normality	Lilliefors normality	Chi-squared normality
Algorithm 1	no	no	no	no	no	no	no	yes
Algorithm 2	no	no	no	no	no	no	no	yes
Algorithm 3	no	no	no	yes	no	no	yes	yes
Algorithm 4	no	no	no	yes	no	no	yes	yes
Algorithm 5	no	no	no	no	no	no	yes	yes
Harrington	no	no	no	yes	no	no	yes	yes

Table 4.3: Results of the normality test over HJC squared error. In the first 5 row the data are from our predictive method, in the last one data are from Harrington's.

As it is possible to see in the above table, this analysis proved that the *squared HJCx,y,z error* in x, y and z direction is most of the time not normally distributed according to Chi-squared test, and never normally distributed according to Lilliefors test. Instead, the *distance* is normally distributed, except for the data obtained with *Algorithms 1* and 2.

Similarly to the previous section, we performed the statistical comparison of our and Harrington's data using a one-sided two-sample Kolmogorv-Smironff test for non-normally distributed data (*squared HJCx,y,z error*) and a one-sided two-sample t-test for normally distributed data (*distance*). While analysing *squared HJCx,y,z errors*, no statistical evidence of improvement was found in x and z direction while, we had statistical evidence of lower error in HJCy estimation at 5% significance level for

STATISTICAL COMPARISON				
	Distanza t-test		Distanza K-S test	
	Is better?	p-value	Is better?	p-value
Algorithm 1	10%	0.053	10%	0.051
Algorithm 2	yes	0.044	yes	0.028
Algorithm 3	yes	0.038	-	-
Algorithm 4	yes	0.372	-	-
Algorithm 5	10 %	0.051	-	-

Table 4.4: Statistical hypothesis tests for the comparison of Harrington's method with ANN. On the distances we performed t-test, and for non normally distributed data, according to Lilliefors test, aslo a Kolmogorov-Smirnoff

Algorithms 2, 3 and *4*, and at 10% significance level for *Algorithms 1* and *5*. Therefore, we performed on *squared HJCx,z error* another Kolmogorov-Smirnoff test with the null hypothesis of data equality and the alternative hypothesis that the Harrington's data have smaller error than ours. This last test never rejected H0, which means we don't have statistical evidence that Harrington's results have smaller errors fr HJCx and HJCy. The t-test on the *distance* parameters proved that only two of the implemented algorithms had statistical evidence, at 5% significance level, to improve HJC localization: *Algorithm 2* and *Algorithm 3*. Between them only *Algorithm 3* proved to provide a better HJC estimation than Harrington's, at 5% significance level, both when used on data from the same dataset they were trained on, and when used on data coming from different datasets. *Algorithm 1* and *Algorithm 5* also proved to have lower distance error than Harrington's, but only at 10% significance level. There was no statistical evidence that *Algorithm 4*, which is the one implemented without gender as input parameter, was improving HJC estimation.

According to the analysis performed here and in the previous section, we consider *Algorithm 3* the best performing among all the algorithms implemented. By applying this algorithm, the mean value of *distance* that is below 9.5mm, which corre-

NORMALITY TEST							
Algorithm	Squared HJCx error		Squared HJCy error		Squared HJCz error		Distance	
	Lilliefors normality	Chi-squared normality	Lilliefors normality	Chi-squared normality	Lilliefors normality	Chi-squared normality	Chi-squared normality	Lilliefors normality
Algorithm 6	no	yes	no	yes	no	yes	yes	yes
Algorithm 7	no	no	no	no	no	yes	yes	yes
Harrington	no	yes	no	yes	no	no	yes	yes

Table 4.5: Results of the normality test over *squared HJCx,y,z error* and *distance*. In the first 2 rows the data are from our predictive method, in the last one data are from Harrington's.

sponds to an improvement compared with Harrington's method of 20%. Similarly to the previous section, there is also a decrease in variance (19%) and in RMS value (17%).

4.1.3 Statistical analysis of noisy data

In section 3.8 fat and skin artefact have been simulated in two different ways (with and without body mass index) and added to the data in Dataset1. The neural networks in this two algorithms have been trained to estimate HJC from noisy data. Then, the two implemented algorithms were applied to a subset of the noisy dataset that wasn't used for training. The statistical analysis was performed on the aforementioned data and the gold standard used for the comparison was Harrington's algorithm applied on Dataset2 without noise addition.

For this datasets we performed the statistical analysis on the *squared HJCx,y,z errors* and on the *distance* parameter. The analysis steps are the same as in the previous section: first, we verified normality of data distribution using Lilliefors and Chi-squared tests, and then we executed the comparison with Harrington's method. The results of the normality tests are in Tab. 4.5.

From normality tests we can deduce that *squared HJCx,y,z errors* are not normally distributed according to Lilliefors test while, according to Chi-squared test,

some of them are normally distributed. Instead, *distance* data proved to be normally distributed according to both Lilliefors and Chi-squared tests.

COMPARISON TEST		
	Distance t-test	
	Is better?	p-value
Algorithm 6	10%	0.095
Algorithm 7	yes	0.050

Table 4.6: Statistical hypothesis tests for the comparison of Harrington's method with ANN with noise simulation. We performed t-test on distances data.

Since *squared HJCx,y,z errors* were non-normally distributed, we performed the Kolmogorov-Smirnoff test. As concerns *distance* data, that we proved to be normal, we used t-test for the comparison. We found statistical evidence of HJCx estimation improvement, but no evidence of estimation improvement in y and z direction. Therefore, as in the previous section, we performed on *squared HJCy,z error* another Kolmogorov-Smirnoff test, with the null hypothesis of data equality and the alternative hypothesis that the Harrington's data have smaller error than ours. For none of the tests the null hypothesis was rejected, meaning that there isn't statistical evidence that our HJCy and HJCz estimation is worse then Harrington's. For the network developed without BMI, we had evidence that, at 10% significance level, the *squared HJCx error* is smaller than the one estimated by Harrington. Instead, while considering the network with BMI index, we get to the same conclusion but with a significance level of 5%. When analysing *distance* data, we had statistical evidence of a smaller *distance* between real and estimated HJC with a 5% significance level for simulation with BMI, and of 10% when BMI was not used. Although the estimation with Harrington algorithm was made without noise addition, our method still proved to localize HJC better. In particular, we have an increase of accuracy in HJCx estimation of 16% (simulation with BMI) and of 13% (simulation without BMI). The improvement in *distance* is of 19% (simulation without BMI) and 25% (simulation with BMI).

4.2 Gender and age factors

In this final part of the statistical analysis on the results we will evaluate if the increase of accuracy that we have obtained by using ANN can be imputed to the introduction of age and gender as input parameters. This analysis was also made in [7], and in this case the authors reached to the conclusion that the utilization of age and gender in predictive HJC estimation was not improving the accuracy of the results.

We started by analysing the differences between the estimation with and without age parameter. The mean and RMS on the error data estimated with the two algorithms were almost equal, with differences of the order of tenths of a millimetre. Therefore, we hypothesised that there was no accuracy difference between the two algorithms. Our prediction was confirmed by the Kolmogorov-Smirnoff test we performed on the *squared error of HJCx,y,z* and also by the t-test and Kolmogorv-Smirnoff we performed on the 3D distances between real and estimated HJC.

Network without gender VS Network with gender									
	Squared HJCx error		Squared HJCy error		Squared HJCz error		t-test on distances		K-S test on distances	
	Is better?	p-value	Is better?	p-value	Is better?	p-value	Is better?	p-value	Is better?	p-value
Accuracy data	no	0.739	no	0.874	no	0.967	-	-	no	0.432
Generalization data	yes	0.015	no	0.976	no	0.906	no	0.103	-	-

Table 4.7: Statistical hypothesis tests for the comparison of *Algorithm 3* (including gender among input parameter) and *Algorithm 4* (not including gender among input parameters). The test on squared HJCx,y,z is Kolmogorov-Smirnoff. On the distances we performed t-test for normally distributed data and Kolmogorov-Smirnoff for the other.

Then we proceed with comparison of the prediction of HJC position with the network without gender among estimation parameters (*Algorithm 4*) and the one with full input parameter (*Algorithm 3*). According to the normality tests on the

data performed in Section 4.1.1 and in Section 4.1.2, we have evidence that there is only one normally distributed dataset among the result. It is the one referred to the parameter *distance*, and only when the ANN is applied to dataset that are not used for the training. While testing for normality the results dataset obtained in Section 3.4, all the *squared HJCx,y,z errors* are not normally distributed, while the two *distance* datasets are. In Tab. 4.7 are reported the results of the comparison test for the accuracy data and generalization data. Accuracy data are the data obtained applying the selected algorithm to the testing subset of Dataset1, while generalization data are obtained by applying the same algorithm to Dataset2 and Dataset3.

If we analyse the accuracy data comparison there seems to be no improvement at all. Instead, when evaluating accuracy of the algorithm while generalising to other datasets, we can spot in the *distance* comparison a p-value of 0.103 (yellow data) and in *squared HJCx estimation* a p-value of 0.015. This result gives statistical evidence that with a 10.3% significance level we can observe a decrease in *distance* between real and estimated HJC, and also a decrease in HJCx estimation at 1.5% significance level. All this is due to the introduction of gender in the input parameters. Moreover, with reference to Tab.4.4, we can see that among all the implemented and tested network the only one that haven't proved to perform better than Harrington's method is the ANN developed without gender as input parameter. We weren't able to demonstrate that the network with full input parameters performs better than the one without gender in both tests, and therefore, we believe that our analysis is not conclusive. Anyway, we think that this results together with the comparison of performance of *Algorithm 4* with Harrington's method indicates that the use of gender should be take into account.

5

Conclusion and further work

In this thesis work, a novel method for estimating the position of the joint articulation centre of the hip for lower limb motion analysis applications was conceived, developed and evaluated. The application we see for this method is in gait pattern analysis of subject with neural or musculoskeletal disabilities. Therefore a suitable method for estimation of HJC should be a predictive one [6]. The best algorithm for predictive HJC estimation is the regression based approach developed by Harrington et al; in their work the regression-based estimation is made on the length of three anatomical parameter: pelvis depth, pelvis width and clinical leg length. The novel estimation method we developed instead was implemented using neural networks, and so it was possible to include a binary data (gender) among input parameter for HJC estimation. Age was also included.

The ANN algorithm has been validated in two distinct phases: on testing subset of Dataset1 (on which the network was trained) and on Dataset2 and Dataset3. In both validation stages, the performance of the algorithm was compared with the accuracy Harrington's method. Then the presence of soft tissue artefacts was simulated noise addition to the original measurements of PW, PD and LL that were made on imaging data. A comparison of our performance with the gold standard for predictive method was also made.

Within the validation phase we evaluate two property of the network: one is accuracy and the other is the accuracy of the algorithm while generalising to other datasets. Among the implemented algorithms the best performing is *Algorithm 3*. The most notable differences between the ANN algorithm and Harrington's can be spotted in the comparison of the distance between real and estimated HJC. For this parameter the accuracy of our method proved to have improved precision of the localization of 20% (accuracy test) and 17% (generalization test). The mean distance was below 6mm and 10mm respectively. The statistical analysis made on HJCx, HJCy and HJCz alone proved no difference among the two methods for HJCz. For HJCx we proved better performance of *Algorithm 3* when applied on testing subset of dataset1, while no evidence of this were found when applied Dataset2 and Dataset3. For HJCy we proved better performance of *Algorithm 3* when applied on Dataset2 and Dataset3, while no evidence of this improvement were found when the algorithm was applied to the testing subset of Dataset1.

The validation of the best performing method was carried out also on data with simulated noise. The noise added was simulated as follows: white noise in range $\pm$ 10mm to PW, random error in range 10mm-38mm to PD and white noise in range $\pm$ 30 to LL . PD was also simulated as 10mm plus random error in range [0,1] and multiplied by BMI. After two new neural network was trained and tested on the noisy data. We compared this results with Harrington's (without noise addiction) and again, analysing the data of distance between real and simulated HJC, we proved that ANN was performing better. The mean distance was slightly above 6mm with an improvement still around 19%. The error was slightly higher for the simulation without BMI.

Our analysis on the importance of including gender as input parameter was not conclusive. Anyway, the obtained data proved a certain correlation between the improvement in HJC localization and the use of gender as input parameter. Therefore, we believe further analysis on this correlation should be conducted.

In this thesis project the neural networks were implemented with supervised

training using data from only one dataset and with a limited amount of data. Since the inference strength of ANNs is related to the quantity, as well as diversity, of the data used in training phase, we believe that more accurate network can be implemented using more data from different datasets. This means that the room for improvement of this method is considerable and could be exploited when new data will be available.

Within this project we have simulated the noise due to soft tissue artefact on the estimation parameter. Due to lack of sterophotogrammetric data in the relative literature, it was not possible to evaluate our algorithm in experimental conditions. This is a common problem to all the papers on predictive methods we analysed in the thesis. Nevertheless, we believe that a comprehensive analysis on experimental data should be enforced, in order to obtain a deeper understanding on the predictive power of our method.

Bibliography

[1] R. Baker, "Gait analysis methods in rehabilitation", *Journal of NeuroEngineering and Rehabilitation*, vol. 3, 2006.

[2] V. Kanawade, L. Dorr, S. Banks, Z. Zhang, and Z. Wan, "Precision of robotic guided instrumentation for acetabular component positioning", *The Journal of Arthroplasty*, vol. 30, pp. 392–397, 2015.

[3] C. Luo, *Reference axes for reconstruction of the knee.* 2004, vol. 11, pp. 251–257.

[4] M. Harrington, A. Zavatskyb, S. Lawsonb, Z. Yuanb, and T. Theologisa, "Prediction of the hip joint centre in adults, children, and patients with cerebral palsy based on magnetic resonance imaging", *Journal of Biomechanics*, vol. 40, pp. 595–602, 2007.

[5] N. Fiorentino, P. Atkinsa, M. Kutschkea, K. B. Foremana, and E. A. A, "In-vivo quantification of dynamic hip joint center errors and soft tissue artifact", *Gait & Posture*, vol. 50, pp. 246–251, 2016.

[6] H. Kainz, C. Carty, L. Modenese, R. Boydd, and D. Lloyd, "Estimation of the hip joint centre in human motion analysis: A systematic review", *Clinical Biomechanics*, vol. 30, pp. 319–329, 2015.

[7] R. Hara, J. McGinley, C. Briggs, R.Baker, and M. Sangeux, "Predicting the location of the hip joint centres, impact of age group and sex", *Scientific Reports*, Nature, Ed., 2016.

[8]   A. Leardini, A. Cappozzo, F. Catani, S. Toksvig-Larsen, A. Petitto, V. Sforza, G. Cassanelli, and S. Giannini, "Validation of a functional method for the estimation of hip joint centre location", *Journal of Biomechanics*, vol. 32, pp. 99–103, 2016.

[9]   M. Sangeuxa, A. Peters, and R. Baker, "Hip joint centre localization: Evaluation on normal subjects in the context of gait analysis", *Gait & Posture*, vol. 34, pp. 324–328, 2011.

[10] A. Cappozzo, U. D. Croce, A. Leardini, and L. Chiari, "Human movement analysis using stereophotogrammetry. part 1: Theoretical background", *Gait & Posture*, vol. 21, pp. 186–196, 2005.

[11] R. Stagni, A. L. A. Cappozzo, M. G. Benedetti, and A. Cappello, "Effects of hip joint centre mislocation on gait analysis results", *Journal of Biomechanics*, vol. 33, pp. 1479–1487, 2000.

[12] R. Baker, A. Esquenazi, M. Benedetti, and K. Desloovere, "Gait analysis: Clinical facts", *European Journal of Physical and Rehabilitation Medicine*, 2016.

[13] A. A. of Orthopedaic Surgeons. (). Total hip replacement, [Online]. Available: https://orthoinfo.aaos.org/en/treatment/total-hip-replacement/.

[14] V. Bouffard, M. Begon, A. Champagne, P. Farhadnia, P. Vendittoli, M. Lavigne, and F. Prince, "Hip joint center localisation: A biomechanical application to hip arthroplasty population", *Word Journal of Orthopaedics*, vol. 3, pp. 131–136, 2012.

[15] G. Lewinnek, J. Lewis, R. Tarr, C. Compere, and J. Zimmerman; "Dislocations after total hip-replacement arthroplasties", *The Journal of Bone & Joint Surgery*, vol. 60, pp. 217–220, 1978.

[16] A. Bell, D.R.Pedersen, and R.A.Brand, "A comparison of the accuracy of several hip center location prediction methods", *Journal of Biomechanics*, vol. 23, pp. 617–621, 1990.

[17] G. Seidel, D. Marchinda, M. Dijkers, and R. Soutas-Little, *Hip joint center location from palpable bony landmarks — A cadaver study.* 1995, vol. 28, pp. 995–998.

[18] K. Halvorsen, M. Lesser, and A. Lundberg, "A new method for estimating the axis of rotation and the center of rotation", *Journal of Biomechanics*, vol. 32, pp. 1221–1227, 1999.

[19] J. Zou, Y. Han, and S. So, *Overview of Artificial Neural Networks. In: Livingstone D.J. (eds) Artificial Neural Networks. Methods in Molecular Biology^{TM}*, H. Press, Ed. 2008, vol. 458, pp. 15–24.

[20] A. Gordon and L. Klebanov, "On a paradoxical property of the kolmogorov–smirnov two-sample test", *IMS Collections*, vol. 7, pp. 70–74, 2010.

[21] F. Burden and D. Winkler, *Bayesian Regularization of Neural Networks. In: Livingstone D.J. (eds) Artificial Neural Networks. Methods in Molecular Biology.* 2008, vol. 458, pp. 25–44.

[22] B. Fischer and P. Mitteroecker, "Covariation between human pelvis shape, stature, and head size alleviates the obstetric dilemma", *Proceedings of the National Academy of Sciences*, vol. 112, pp. 5655–5660, 2015.

[23] A. Leong, "Sexual dimorphism of the pelvic architecture: A struggling response to destructive and parsimonious forces by natural & mate selection.", *McGill Journal of Medicine*, vol. 9, pp. 61–66, 2006.

[24] P. Secombe, R. Sutherland, and R. Johnson, "Body mass index and thoracic subcutaneous adipose tissue depth: Possible implications for adequacy of chest compressions", *BMC Research Notes*, 2017.

[25] B. Bogin and M. I. Varela-Silva, "Leg length, body proportion, and health: A review with a note on beauty", *International Journal of Environmental Research and Public Health*, vol. 7, pp. 1047–1075, 2010.

[26] A. Peters, B. Galna, M. Sangeux, M. Morris, and R. Baker, "Quantification of soft tissue artifact in lower limb human motion analysis: A systematic review", *Gait and Posture*, vol. 31, pp. 1–8, 2010.

[27] M. Sangeux, "On the implementation of predictive methods to locate the hip joint centres", *Gait and Posture*, vol. 42, pp. 402–405, 2015.

[28]   R. Davis, S. Ounpuu, D. Tyburski, and J.R.Gage, "A gait analysis data collection and reduction technique", *Human Movement Science*, vol. 10, pp. 575–587, 1991.

<div align="right">

A

</div>

Used dataset

The three full datasets used for the development of this project are reported below. The first one is **Dataset1** from Hara et al.[7]. In the column there are fifteen elements:

- KEY: unique number to represent the individual

- AGE: age

- GROUP (3): age group with 3 categories: children 1, adolescents 1 and adults 3

- GROUP (2): age group with 2 categories: children C and skeletally matured A

- SEX: Male or Female

- SIDE: Right or Left

- Inter ASIS distance (mm): distance between the left and right ASIS

- Clinical Leg Length (mm): leg length, measured from ASIS to medial epicondyle of the knee, then to medial malleola

- Total Pelvic Width (mm): distance between the two most lateral points of the pelvis (edge of the iliac crest)

- Pelvic Depth (mm): distance between the ASIS midpoint and the PSIS midpoint

- Height (mm): height, measured on the CT table

- Weight (kg): weight, measured on the CT table

- HJCx (mm): X (antero-posterior) position of the hip joint centre

- HJCy (mm): Y (lateral-medial) position of the hip joint centre

- HJCz (mm): Z (up-down) position of the hip joint centre

KEY	AGE	GROUP (3)	GROUP (2)	SEX	SIDE	Inter ASIS distance (mm)	Clinical Leg Length (mm)	Total Pelvic Width (mm)	Pelvic Depth (mm)	Height (mm)	Weight (Kg)	HJCx (mm)	HJCy (mm)	HJCz (mm)
1101	5	1	C	M	R	156.1	476.8	169.4	64.9	1040	17	-12.4	48.7	-45.4
1102	5	1	C	M	R	154.3	524.5	173.9	77.4	1000	22	-18.0	53.5	-47.8
1103	5	1	C	M	R	145.9	511.9	161.0	77.3	1050	18	-22.0	51.3	-51.2
1104	5	1	C	M	R	139.7	551.9	166.1	83.6	1160	17	-27.6	55.6	-54.4
1105	5	1	C	M	R	153.1	539.3	178.5	80.9	1160	26	-27.0	54.9	-49.6
1106	9	1	C	M	R	183.7	675.0	200.2	89.7	1380	38	-21.3	66.0	-64.0
1107	6	1	C	M	R	154.6	550.7	172.6	78.7	1130	23	-16.9	53.2	-53.4
1108	5	1	C	M	R	171.0	547.5	191.1	81.2	1170	28	-14.7	59.1	-54.8
1109	9	1	C	M	R	169.1	748.7	200.4	108.5	1470	36	-40.9	65.7	-61.7
1111	6	1	C	M	R	158.7	585.5	189.0	89.8	1190	22	-30.2	58.8	-55.8
1112	9	1	C	M	R	177.2	684.0	202.1	97.5	1350	38	-32.4	61.4	-61.8
1113	5	1	C	M	R	147.2	507.3	168.0	80.0	1040	17	-24.1	50.8	-45.6
1114	8	1	C	M	R	190.9	722.3	216.8	102.0	1410	44	-34.9	66.3	-62.3
1115	6	1	C	M	R	181.8	633.8	200.4	88.5	1300	34	-21.7	61.2	-59.8
1116	5	1	C	M	R	161.0	534.5	180.5	81.3	1110	26	-23.8	57.8	-50.6
1117	6	1	C	M	R	138.2	555.8	162.8	78.7	1120	21	-25.8	55.6	-51.1
1118	8	1	C	M	R	181.1	631.9	197.6	86.9	1290	23	-23.2	62.0	-62.4
1119	11	1	C	M	R	225.3	817.3	260.1	120.3	1700	77	-41.2	76.4	-74.5
1120	5	1	C	M	R	144.3	510.4	162.3	73.1	1070	20	-24.3	53.1	-48.5
1121	5	1	C	M	R	153.6	510.0	177.7	77.1	1100	23	-19.9	55.5	-52.1
1122	5	1	C	M	R	144.3	505.3	163.8	69.9	1050	16	-20.6	48.4	-51.6
1123	9	1	C	M	R	166.8	695.8	193.6	94.3	1330	29	-29.3	57.5	-59.7
1124	10	1	C	M	R	223.0	778.9	247.9	104.9	1520	70	-22.8	70.2	-69.8
1125	10	1	C	M	R	175.5	728.6	208.5	106.9	1490	35	-33.9	69.1	-61.9
1201	5	1	C	F	R	139.7	526.5	159.2	80.7	1110	19	-28.9	53.9	-52.5
1202	11	1	C	F	R	170.9	680.0	198.7	100.7	1350	26	-38.0	64.0	-62.0
1203	11	1	C	F	R	199.8	735.7	229.4	109.8	1480	65	-33.8	66.6	-61.9
1204	11	1	C	F	R	196.6	738.6	225.9	123.2	1400	40	-41.3	78.1	-67.3
1205	11	1	C	F	R	224.5	780.2	240.3	107.7	1490	67	-34.9	75.8	-75.7
1206	7	1	C	F	R	148.7	617.8	175.7	86.0	1210	20	-31.3	54.1	-58.1
1207	10	1	C	F	R	198.0	748.4	223.6	111.0	1470	61	-31.3	66.2	-60.9
1208	9	1	C	F	R	174.2	665.8	200.5	92.5	1320	27	-31.3	59.5	-57.9
1209	9	1	C	F	R	174.9	765.7	199.4	95.6	1560	53	-38.0	60.3	-65.6
1210	8	1	C	F	R	177.0	660.0	201.2	91.7	1350	30	-28.2	60.1	-57.7
1211	8	1	C	F	R	174.7	673.4	204.2	94.1	1310	33	-27.5	59.1	-56.1
1212	8	1	C	F	R	166.8	605.0	184.4	87.7	1210	27	-24.4	59.5	-54.2
1213	7	1	C	F	R	161.1	651.2	183.8	83.6	1230	23	-28.6	53.8	-58.9
2101	17	2	A	M	R	222.5	873.1	264.9	136.2	1720	82	-37.2	80.1	-76.9
2102	18	2	A	M	R	234.2	871.5	273.0	143.2	1680	59	-47.8	79.4	-84.8

KEY	AGE	GROUP (3)	GROUP (2)	SEX	SIDE	Inter ASIS distance (mm)	Clinical Leg Length (mm)	Total Pelvic Width (mm)	Pelvic Depth (mm)	Height (mm)	Weight (Kg)	HJCx (mm)	HJCy (mm)	HJCz (mm)
2103	19	2	A	M	R	198.1	907.1	264.1	151.7	1780	64	-55.7	87.3	-83.9
2104	16	2	A	M	R	242.0	812.8	277.8	126.4	1710	96	-24.8	82.7	-83.9
2105	16	2	A	M	R	202.1	855.4	231.5	123.5	1660	55	-52.2	76.4	-70.5
2106	19	2	A	M	R	227.8	891.7	272.6	140.1	1730	67	-42.7	80.3	-76.7
2107	19	2	A	M	R	217.2	868.8	255.3	138.4	1650	71	-33.5	84.7	-82.7
2108	19	2	A	M	R	231.3	901.2	261.1	132.1	1690	63	-37.2	76.0	-89.0
2109	16	2	A	M	R	225.6	902.9	287.5	146.9	1700	91	-40.0	80.5	-80.6
2110	17	2	A	M	R	214.4	875.6	271.6	142.6	1700	81	-55.2	82.7	-79.6
2111	18	2	A	M	R	185.2	922.2	240.9	148.3	1760	66	-59.2	86.5	-76.8
2112	16	2	A	M	R	242.9	882.1	272.8	142.8	1720	70	-37.4	82.1	-85.7
2113	17	2	A	M	R	199.7	866.7	265.5	143.5	1730	61	-47.6	84.1	-82.6
2114	19	2	A	M	R	201.5	910.2	265.7	157.9	1780	82	-57.3	86.2	-81.5
2115	17	2	A	M	R	216.6	908.1	250.6	145.5	1700	59	-44.1	82.4	-72.6
2116	16	2	A	M	R	235.5	951.2	270.6	144.0	1730	57	-41.8	78.9	-83.3
2117	17	2	A	M	R	226.2	918.7	264.9	139.2	1800	63	-50.6	82.0	-82.7
2118	18	2	A	M	R	203.0	827.1	266.0	145.4	1630	81	-45.3	81.7	-80.9
2119	19	2	A	M	R	263.4	965.9	293.5	145.8	1860	80	-36.3	86.7	-78.8
2120	18	2	A	M	R	217.4	958.8	265.9	155.3	1800	59	-49.6	82.8	-74.7
2121	19	2	A	M	R	198.8	947.9	243.5	142.2	1760	74	-41.9	80.9	-77.7
2122	17	2	A	M	R	208.7	893.3	257.6	148.3	1710	78	-52.7	85.8	-78.7
2123	19	2	A	M	R	226.1	859.4	270.1	150.3	1720	108	-50.1	81.2	-73.7
2124	17	2	A	M	R	236.3	942.5	275.9	137.7	1700	57	-44.9	86.5	-79.7
2125	19	2	A	M	R	231.7	866.7	259.9	145.1	1700	64	-38.1	77.7	-66.8
2126	18	2	A	M	R	248.2	869.4	278.4	127.0	1660	87	-37.8	76.5	-79.9
2127	19	2	A	M	R	223.3	959.4	275.5	151.5	1820	74	-56.3	87.4	-83.6
2128	19	2	A	M	R	200.0	923.7	218.5	119.3	1700	54	-34.3	68.8	-74.3
2129	18	2	A	M	R	230.9	893.8	270.1	140.2	1670	60	-41.3	81.1	-75.6
2130	18	2	A	M	R	221.7	843.0	261.7	128.6	1640	53	-45.0	80.7	-82.1
2201	18	2	A	F	R	159.1	850.8	214.0	148.4	1630	55	-48.6	79.0	-81.1
2202	17	2	A	F	R	187.6	819.3	222.9	149.9	1620	53	-50.9	82.1	-72.8
2203	18	2	A	F	R	209.9	816.8	255.9	143.9	1580	73	-49.4	86.1	-85.9
2204	19	2	A	F	R	209.9	811.3	251.0	136.8	1540	57	-38.9	78.0	-73.6
2205	19	2	A	F	R	197.5	792.3	226.6	127.0	1540	68	-33.3	78.3	-80.4
2206	17	2	A	F	R	215.7	820.4	255.2	141.9	1610	52	-50.2	83.8	-75.8
2207	16	2	A	F	R	211.6	881.8	259.4	152.8	1690	54	-52.2	81.2	-77.2
2208	17	2	A	F	R	215.5	847.5	268.3	146.3	1730	64	-46.3	87.2	-76.8
2209	17	2	A	F	R	191.2	815.6	240.3	136.1	1610	60	-39.4	82.9	-82.6
2210	19	2	A	F	R	187.4	836.4	239.2	142.6	1580	64	-43.6	78.2	-84.1
2211	18	2	A	F	R	255.7	834.5	288.8	149.3	1640	112	-39.9	86.9	-72.8
2212	18	2	A	F	R	213.9	814.4	250.1	131.7	1610	52	-36.0	85.0	-76.2
2213	16	2	A	F	R	205.5	850.8	254.8	137.4	1680	57	-47.6	85.9	-61.7
2214	16	2	A	F	R	202.2	845.1	238.4	136.0	1650	54	-46.0	80.1	-78.4
2215	16	2	A	F	R	231.5	893.4	265.2	145.4	1710	64	-52.7	88.6	-82.3
2216	19	2	A	F	R	214.7	814.9	263.8	137.6	1650	73	-43.3	82.9	-75.2
2217	16	2	A	F	R	226.2	890.1	266.8	145.9	1570	53	-50.3	81.6	-80.2
2218	18	2	A	F	R	243.5	910.4	284.8	136.2	1690	54	-41.8	90.7	-82.6
2219	18	2	A	F	R	207.8	815.7	255.5	144.1	1650	74	-44.1	82.5	-77.5
2220	18	2	A	F	R	204.8	886.0	262.0	138.4	1660	53	-43.4	83.6	-78.7
2221	17	2	A	F	R	213.1	860.9	257.5	141.8	1660	53	-53.5	88.3	-85.5
2222	17	2	A	F	R	228.5	885.8	260.0	137.1	1640	57	-36.9	84.4	-82.7
2223	18	2	A	F	R	219.6	920.6	277.4	162.4	1730	63	-62.0	81.3	-82.6
2224	19	2	A	F	R	208.8	843.2	245.5	137.2	1640	63	-41.5	77.4	-73.2
2225	17	2	A	F	R	228.0	876.0	274.7	147.6	1720	57	-50.3	85.9	-77.2
2226	19	2	A	F	R	204.2	799.3	244.3	136.9	1550	52	-43.3	81.0	-66.2
2227	17	2	A	F	R	191.2	847.0	247.6	142.8	1630	49	-47.9	78.8	-75.4
2228	17	2	A	F	R	213.3	816.7	271.0	140.1	1600	73	-42.4	80.2	-74.3

KEY	AGE	GROUP (3)	GROUP (2)	SEX	SIDE	Inter ASIS distance (mm)	Clinical Leg Length (mm)	Total Pelvic Width (mm)	Pelvic Depth (mm)	Height (mm)	Weight (Kg)	HJCx (mm)	HJCy (mm)	HJCz (mm)
2229	19	2	A	F	R	220.7	896.4	267.7	144.1	1700	66	-54.2	87.9	-80.5
2230	16	2	A	F	R	214.0	788.9	246.4	133.4	1500	51	-39.9	75.0	-72.8
3101	39	3	A	M	R	238.4	898.8	274.3	133.0	1750	62	-28.3	80.4	-75.0
3102	25	3	A	M	R	220.2	824.9	257.7	130.8	1640	61	-39.4	82.6	-71.9
3103	29	3	A	M	R	211.8	849.5	260.6	142.2	1650	81	-43.7	84.4	-75.4
3104	33	3	A	M	R	225.9	923.0	270.7	142.1	1760	95	-36.0	86.1	-85.3
3105	31	3	A	M	R	230.6	871.7	272.0	151.7	1770	80	-48.9	95.0	-84.3
3106	25	3	A	M	R	211.0	819.5	261.1	146.5	1640	67	-45.3	81.7	-72.1
3107	37	3	A	M	R	197.0	853.4	255.1	152.5	1670	103	-53.6	86.7	-80.6
3108	36	3	A	M	R	242.4	885.4	291.7	148.6	1700	107	-41.3	80.7	-80.8
3109	35	3	A	M	R	260.9	883.7	296.3	137.1	1710	77	-41.6	88.1	-80.7
3110	28	3	A	M	R	230.0	888.6	270.5	139.7	1730	70	-45.6	83.7	-81.4
3111	31	3	A	M	R	224.8	839.6	259.1	136.1	1660	70	-42.5	82.2	-78.3
3112	31	3	A	M	R	234.3	947.8	260.5	142.4	1780	58	-47.4	88.0	-83.4
3113	40	3	A	M	R	220.1	982.2	270.9	161.6	1890	123	-56.8	97.1	-85.5
3114	28	3	A	M	R	224.3	881.5	260.6	151.5	1700	67	-48.7	90.9	-69.0
3115	34	3	A	M	R	247.3	958.1	282.0	149.6	1840	70	-49.5	96.6	-86.2
3116	35	3	A	M	R	194.4	786.0	223.8	128.0	1550	74	-49.0	75.2	-72.3
3117	30	3	A	M	R	223.0	892.5	263.9	121.2	1700	73	-37.5	81.2	-72.6
3118	31	3	A	M	R	224.2	925.9	284.9	153.2	1750	65	-43.6	95.4	-85.6
3119	26	3	A	M	R	243.3	852.2	277.1	135.9	1710	62	-43.6	87.7	-76.2
3120	32	3	A	M	R	255.5	964.0	296.2	150.5	1840	90	-53.3	94.6	-87.2
3121	38	3	A	M	R	224.3	927.6	262.9	149.6	1740	84	-50.9	89.2	-88.8
3122	25	3	A	M	R	242.5	953.2	288.6	143.6	1840	135	-41.4	94.3	-88.8
3123	27	3	A	M	R	199.8	992.2	261.1	148.1	1840	76	-41.7	86.7	-80.1
3124	25	3	A	M	R	239.8	1045.7	293.1	162.3	1900	78	-52.1	88.0	-88.7
3125	32	3	A	M	R	229.2	864.1	301.7	153.4	1690	79	-54.5	89.1	-80.7
3126	39	3	A	M	R	232.9	896.0	261.4	145.8	1710	93	-37.0	88.7	-75.1
3127	37	3	A	M	R	252.2	993.8	296.9	152.6	1880	121	-51.1	96.9	-91.9
3128	29	3	A	M	R	243.2	955.5	280.4	130.3	1730	77	-41.2	83.7	-77.8
3129	26	3	A	M	R	245.9	941.6	290.0	149.6	1800	86	-38.6	83.6	-81.4
3130	29	3	A	M	R	229.2	937.2	270.3	157.0	1800	88	-45.6	80.3	-82.6
3201	25	3	A	F	R	220.7	905.7	271.3	157.1	1700	107	-59.8	88.9	-88.6
3202	35	3	A	F	R	244.9	827.9	275.4	132.8	1610	84	-46.9	87.4	-80.5
3203	31	3	A	F	R	221.7	855.4	267.3	140.4	1650	52	-46.0	81.7	-79.0
3204	30	3	A	F	R	224.7	799.5	249.1	126.1	1510	44	-43.6	84.3	-62.3
3205	37	3	A	F	R	200.7	802.7	259.3	145.1	1580	67	-49.8	82.4	-73.2
3206	28	3	A	F	R	228.4	806.9	277.8	147.0	1620	59	-43.4	91.4	-71.8
3207	29	3	A	F	R	229.4	875.0	271.3	146.2	1670	68	-42.8	85.9	-82.0
3208	35	3	A	F	R	222.0	776.7	272.7	150.0	1560	109	-44.5	90.2	-76.2
3209	34	3	A	F	R	200.3	877.8	241.4	138.6	1570	52	-44.8	88.2	-73.1
3210	38	3	A	F	R	210.2	875.5	259.2	145.5	1720	69	-44.5	93.8	-91.7
3211	35	3	A	F	R	248.7	820.9	275.2	131.3	1580	94	-27.6	83.4	-80.6
3212	37	3	A	F	R	216.1	904.2	248.5	122.3	1610	56	-40.2	81.1	-73.7
3213	38	3	A	F	R	198.4	820.8	265.2	151.0	1620	89	-39.6	86.7	-68.3
3214	29	3	A	F	R	236.9	823.4	277.0	136.2	1600	57	-40.1	88.3	-71.3
3215	30	3	A	F	R	213.6	806.5	261.1	142.9	1650	97	-47.9	83.7	-74.1
3216	25	3	A	F	R	216.1	758.0	255.9	129.0	1500	51	-37.8	74.0	-64.3
3217	33	3	A	F	R	200.9	870.4	275.2	149.4	1710	76	-53.9	95.1	-83.7
3218	31	3	A	F	R	252.2	832.3	291.9	137.3	1660	72	-37.3	86.4	-75.2
3219	25	3	A	F	R	248.7	893.7	294.5	142.8	1700	79	-46.6	86.5	-76.3
3220	39	3	A	F	R	224.0	897.6	289.1	156.1	1700	87	-58.0	94.6	-78.7
3221	25	3	A	F	R	192.2	796.0	231.6	134.0	1570	67	-44.0	77.7	-75.9
3222	33	3	A	F	R	219.3	776.5	270.4	137.1	1570	50	-40.0	79.0	-73.0
3223	38	3	A	F	R	259.1	877.4	288.4	141.7	1630	58	-44.0	82.6	-74.0
3224	29	3	A	F	R	217.7	820.8	258.7	143.4	1600	53	-37.4	77.7	-68.4

KEY	AGE	GROUP (3)	GROUP (2)	SEX	SIDE	Inter ASIS distance (mm)	Clinical Leg Length (mm)	Total Pelvic Width (mm)	Pelvic Depth (mm)	Height (mm)	Weight (Kg)	HJCx (mm)	HJCy (mm)	HJCz (mm)
3225	31	3	A	F	R	233.9	911.8	286.9	150.7	1690	72	-46.1	86.4	-75.9
3226	29	3	A	F	R	255.0	879.7	299.0	155.3	1700	65	-51.6	94.2	-85.0
3227	40	3	A	F	R	210.7	802.4	273.0	129.8	1550	85	-46.7	79.5	-78.2
3228	39	3	A	F	R	198.8	849.4	264.0	159.7	1610	83	-49.3	96.6	-73.3
3229	37	3	A	F	R	244.7	938.3	271.3	147.0	1770	111	-45.4	88.7	-76.2
3230	36	3	A	F	R	227.7	820.0	274.4	151.8	1640	61	-43.5	92.0	-71.8

Dataset2 is from Harrington et al. [4]. The column elements represents the following data:

- Subject: H: healthy child, A: adult, C: child with cerebral palsy

- Sex: Male or Female

- Age: age

- Mass: weight measured in kg

- H: height in mm

- Leg Length: leg length measured in mm

- D: antero/posterior component of the distance between a point approximating the hip centre and the homolateral ASIS;

- PD: distance between the ASIS midpoint and the PSIS midpoint

- PW: distance between the left and right ASIS

- HJCx: X (antero-posterior) position of the hip joint centre

- HJCy: Z (up-down) position of the hip joint centre

- HJCz: Y (lateral-medial) position of the hip joint centre

Subject	Sex	Age (yrs)	Mass (kg)	PW (mm)	PD (mm)	Leg Length (mm)	HJCx (mm)	HJCy (mm)	HJCz (mm)
H1	M	5.9	20	158.9	89.1	535	-24.50	-47.90	58.50
H2	M	6	21.5	171.2	96.2	602.5	-23.70	-58.30	60.10
H3	M	6	15.5	140.6	81	500	-26.10	-53.10	52.20
H4	F	6.1	21.5	156.2	97.3	612.5	-31.90	-60.60	60.00
H5	F	6.4	23	162.5	100.7	610	-28.00	-69.50	59.20
H6	F	8.1	22.5	171.8	93.7	695.5	-23.70	-65.40	62.80
H7	M	8.3	32	203.2	95	750	-34.60	-66.50	66.00
H8	F	8.5	27.5	181.5	106.3	687.5	-43.30	-64.00	61.80
H9	F	9.6	30	189.1	109.7	795.5	-33.90	-72.70	63.70
H10	M	9.8	34.5	173.4	110.2	785	-41.20	-69.30	64.50
H11	F	10.1	34	171	113.5	730	-37.90	-68.50	60.80
H12	M	11.4	36.5	213.2	103.8	780.5	-40.60	-78.10	75.90
H13	F	12.3	47	215	125	847.5	-48.70	-75.60	78.60
H14	M	13	44	228.2	121.3	880	-36.40	-79.70	72.40
A1	F	22.9	54	205.5	138.9	810	-41.40	-73.90	85.60
A2	M	24.1	79	275.6	163.2	980	-48.10	-91.80	96.10
A3	M	26.1	72.5	246.1	155.8	955	-43.60	-81.90	88.90
A4	F	27	69	231.5	152.5	920	-39.60	-86.60	94.60
A5	M	28.1	75	238.6	152.7	950	-49.70	-90.40	90.10
A6	F	32.6	56	238.4	142.5	865	-51.10	-88.20	86.10
A7	M	33.7	76.5	249.4	145.5	985	-33.40	-82.30	91.90
A8	M	40.1	81	276.1	164.2	950	-51.80	-95.20	95.70
C1	M	6.1	20.5	156.8	92.9	580	-37.20	-53.50	61.50
C2	M	8	20	149.9	91.7	580	-32.80	-57.40	57.20
C3	F	8.2	25	157.2	98.9	660	-37.10	-56.70	62.90
C4	F	8.3	22.5	180.1	83.1	630	-28.20	-59.90	60.90
C5	F	9.1	35	187.4	98	715	-22.90	-70.90	63.70
C6	F	10.6	30	160	102.5	700	-46.00	-65.20	68.00
C7	M	11.4	40	175.3	111.5	745	-40.30	-63.10	66.80
C8	F	11.5	27	182.1	106.1	730	-43.10	-64.60	73.40
C9	M	12.4	40	182.2	112	770	-33.70	-66.40	65.60
C10	M	12.5	29.5	188	90.6	700	-34.50	-67.50	70.10

Dataset3 is from Leardini et al. [8].

- Subject: number associated to a subject

- Sex: Male or Female

- Age: age

- Mass: weight measured in kg

- PW: distance between the left and right ASIS

- PD: distance between the ASIS midpoint and the PSIS midpoint

Subject	Age (yrs)	Mass (kg)	H (mm)	L (mm)	D (mm)	PD (mm)	PW (mm)	HJCx (mm)	HJCy (mm)	HJCz (mm)
1	42	80	1945	1015	73	173	245	-60.8	-100.1	96.8
2	33	70	1840	960	50	159	258	-43.2	-90.1	86.1
3	29	72	1815	975	55	151	241	-46.6	-91.6	78
4	26	74	1730	875	93	170	203	-45.4	-96.6	83.3
5	26	71	1775	940	87	157	242	-53.4	-92.5	84.2
6	20	59	1705	870	73	170	202	-51.9	-80	94.5
7	35	77	1760	840	76	178	231	-54.1	-72.1	86.1
8	27	84	1865	950	77	138	242	-43.2	-81.5	89.6
9	29	84	1850	1005	54	191	250	-61.8	-109.3	92.7
10	26	93	1740	880	45	185	231	-57.1	-87.6	95.9
11	29	77	1735	900	69	178	235	-47.6	-87.5	82.9

- Leg Length: measured from ASIS to medial epicondyle of the knee, then to medial malleola

- HJCx: X (antero-posterior) position of the hip joint centre

- HJCy: Z (up-down) position of the hip joint centre

- HJCz: Y (lateral-medial) position of the hip joint centre